

An Extended Primal-Dual Algorithm Framework for Nonconvex Problems with Application to Nonlinear Imaging

Yu Gao^{*}, Xiaochuan Pan[†], and Chong Chen[‡]

Abstract. We propose an extended primal-dual algorithm framework for solving a general nonconvex optimization model. This work is motivated by image reconstruction problems in a class of nonlinear imaging, where the forward operator can be formulated as a nonlinear convex function with respect to the reconstructed image. Using the proposed framework, we put forward six specific iterative schemes, and present their detailed mathematical explanation. We also establish the relationship to existing algorithms. Moreover, under proper assumptions, we analyze the convergence of the schemes for the general model when the optimal dual variable regarding the nonlinear operator is non-vanishing. As a representative, the image reconstruction for spectral computed tomography is used to demonstrate the effectiveness of the proposed algorithm framework. By special properties of the concrete problem, we further prove the convergence of these customized schemes when the optimal dual variable regarding the nonlinear operator is vanishing. Finally, the numerical experiments show that the proposed algorithm has good performance on image reconstruction for various data with non-standard scanning configuration.

Key words. extended primal-dual algorithm, nonconvex sparse optimization, convex forward operator, image reconstruction, nonlinear inverse imaging problems

AMS subject classifications. 65R32, 68U10, 92C55, 94A08

1. Introduction. We consider image reconstruction problems given as nonlinear operator equations

$$(1.1) \quad \mathbf{g} = \mathbf{K}(\mathbf{f}) + \mathbf{g}_{\text{noise}},$$

where $\mathbf{K} : \mathcal{X} \rightarrow \mathcal{Y}_{\mathbf{K}}$ denotes a Fréchet differentiable nonlinear operator, $\mathbf{f} \in \Omega \subset \mathcal{X}$ is the image to be reconstructed, $\mathbf{g} \in \mathcal{Y}_{\mathbf{K}}$ is measured data, and $\mathbf{g}_{\text{noise}} \in \mathcal{Y}_{\mathbf{K}}$ is uncertain noise. Here \mathcal{X} and $\mathcal{Y}_{\mathbf{K}}$ are two finite-dimensional real vector spaces equipped with an inner product $\langle \cdot, \cdot \rangle$ and norm $\|\cdot\| = \sqrt{\langle \cdot, \cdot \rangle}$, and Ω is a closed convex subset of \mathcal{X} .

Specifically, in spectral computed tomography (CT), for instance, the component of forward projection operator can be formulated as the form of log-sum exponential functional via basis material decomposition [1, 17],

$$(1.2) \quad K_j(\mathbf{f}) := \ln \sum_{m=1}^M s_{jm} \exp\left(-\sum_{d=1}^D b_{dm} \mathbf{a}_j^{\top} \mathbf{f}_d\right),$$

where $\mathbf{K} := [K_1, \dots, K_J]^{\top}$, s_{jm} is the discrete normalized X-ray spectrum at energy bin m for ray j with $\sum_{m=1}^M s_{jm} = 1$, b_{dm} is the decomposition coefficient at energy bin m of the d -th basis

^{*}LSEC, ICMSEC, Academy of Mathematics and Systems Science, Chinese Academy of Sciences, Beijing 100190, China. School of Mathematical Sciences, University of Chinese Academy of Sciences, Beijing 100049, China.

[†]Department of Radiology, The University of Chicago, Chicago, IL 60637, USA.

[‡]LSEC, ICMSEC, Academy of Mathematics and Systems Science, Chinese Academy of Sciences, Beijing 100190, China. School of Mathematical Sciences, University of Chinese Academy of Sciences, Beijing 100049, China.

material, \mathbf{f}_d is the unknown density (image) of the d -th basis material, \mathbf{a}_j is the discrete X-ray transform determined by ray j , and T denotes transpose. For digital breast tomosynthesis (DBT), the functional of form (1.2) is applied as the component of forward projection operator as well [16]. Moreover, for the discrete X-ray transform with nonlinear partial volume effect [5], the component of \mathbf{K} can be represented as

$$(1.3) \quad K_j(\mathbf{f}) := \ln \frac{1}{N_j} \sum_{l_j=1}^{N_j} \exp(-\mathbf{a}_{l_j}^{\mathsf{T}} \mathbf{f}),$$

where N_j denotes the considered total number of rays between detector bin j and focal spot. On the other hand, the component of \mathbf{K} in phase retrieval can be written as

$$(1.4) \quad K_j(\mathbf{f}) := |\langle \mathbf{a}_j, \mathbf{f} \rangle|^2 = \mathbf{f}^{\mathsf{H}} \mathbf{a}_j \mathbf{a}_j^{\mathsf{H}} \mathbf{f},$$

where \mathbf{f} and \mathbf{a}_j are complex vectors, and H denotes conjugate transpose [22].

The image reconstruction problem of interest is to determine unknown \mathbf{f} from measured data \mathbf{g} as in (1.1), where the data is often sparse sampled and/or contains uncertain noise. Generally, solving nonlinear system of the form

$$(1.5) \quad \mathbf{K}(\mathbf{f}) = \mathbf{g}$$

is equivalent to solve an ill-posed inverse problem since the solutions of (1.5) do not depend continuously on the data [15]. An extended algebraic reconstruction technique (EART) was proposed to solve (1.5) for image reconstruction in dual spectral CT (DECT) in [25], which is actually a generalization of algebraic reconstruction technique (ART) or Kaczmarz method for solving linear system to the nonlinear case in (1.5). Similarly, a stochastic gradient descent method was employed and analyzed to solve (1.5) in [14]. The authors in [16] reformulated the image reconstruction problem in (1.5) for DBT as a nonlinear least square problem, and proposed a limited memory BFGS method. Moreover, there are several iterative regularization methods that were developed to solve (1.5), such as nonlinear Landweber iteration, and Newton type methods (see [12, 15] and the references therein). However, few of these literatures considered a regularization term, let alone a nonsmooth one.

The image reconstruction problem in (1.1) can be reformulated as the following constrained optimization problem

$$(1.6) \quad \min_{\mathbf{f} \in \Omega} \left\{ \mathcal{D}(\mathbf{K}(\mathbf{f}), \mathbf{g}) + \mathcal{R}(\mathbf{f}) \right\}.$$

Here $\mathcal{D}(\cdot, \cdot)$ denotes the data fidelity term which is often designed as the form of ℓ_p -norm or Kullback–Leibler (KL) divergence, and $\mathcal{R}(\cdot)$ stands for the regularization term which is frequently schemed as ℓ_1 -norm of the sparse representation of the image under certain basis functions [10]. Generally, it can be written as

$$(1.7) \quad \mathcal{R}(\mathbf{f}) := \lambda \phi(A\mathbf{f}),$$

where $A : \mathcal{X} \rightarrow \mathcal{Y}_A$ is a continuous linear operator and denotes the associated discrete form of the sparse representation, \mathcal{Y}_A is also a finite-dimensional real vector space, and λ is a

nonnegative regularization parameter. Hence, a general nonconvex optimization model can be represented as minimizing a sum of three terms of the form

$$(1.8) \quad \min_{\mathbf{f} \in \mathcal{X}} \left\{ F(\mathbf{K}(\mathbf{f})) + E(A\mathbf{f}) + G(\mathbf{f}) \right\},$$

where each component of \mathbf{K} and A are nonlinear and linear with regard to \mathbf{f} respectively. Note that we do not merge the first two terms in (1.8) into a single one as the model studied in [20], which can help us to focus on the specific term regarding the nonlinear forward operator. For example in (1.6), we can let $F(\cdot) := \mathcal{D}(\cdot, \mathbf{g})$, $E(\cdot) := \lambda\phi(\cdot)$ by (1.7), and

$$G(\mathbf{f}) := \delta_{\Omega}(\mathbf{f}) = \begin{cases} 0 & \text{if } \mathbf{f} \in \Omega, \\ +\infty & \text{otherwise.} \end{cases}$$

Model (1.8) can be also seen as a generalization of the following well-studied convex optimization problem (see [11, 4, 13])

$$(1.9) \quad \min_{\mathbf{f} \in \mathcal{X}} \left\{ E(A\mathbf{f}) + G(\mathbf{f}) \right\}.$$

If \mathbf{K} is linear, model (1.8) boils down to model (1.9). Even though both F and \mathbf{K} are nonlinear convex, their composition $F \circ \mathbf{K}$ is not definitely convex. It is difficult to solve the nonconvex problem as in (1.8). However, there are already some studies on how to solve such kind of problems. For instance, an exact/linearized nonlinear primal-dual hybrid gradient method (PDHGM) was proposed and analyzed in [20, 9], which is a natural extension of the modified PDHGM for solving (1.9) the linear case in [4]. Particularly, the authors in [5, 7] proposed an interesting nonconvex primal-dual algorithm for image reconstruction in spectral CT and discrete X-ray transform with nonlinear partial volume effect. A nonconvex alternating direction method of multipliers (ADMM) was proposed in [2] to solve the nonconvex and possibly nonsmooth optimization problem with application to CT imaging (see [23]). But very few of existing literatures excavate the properties of forward operator \mathbf{K} .

In this work, we focus on solving a class of nonconvex problems in (1.8) with operator \mathbf{K} being nonlinear convex with respect to \mathbf{f} , which is motivated by several practical nonlinear imaging problems with such kind of forward operators. For example, it is easy to verify that K_j in (1.2)–(1.4) are convex with respect to \mathbf{f} . The operator convexity would be useful to develop a framework of extended primal-dual algorithm for these nonconvex problems.

The outline of this paper is organized as follows. Section 2 introduces the required mathematical preliminaries. We propose a framework of extended primal-dual algorithm for nonconvex problems, and establish the relationship to existing algorithms in section 3. The associated convergence is analyzed in section 4. In section 5, we apply the proposed algorithm framework to reconstruct image in spectral CT, and also give the customized analysis and several numerical experiments. Finally, the paper is concluded by section 6.

2. Preliminaries. We introduce Legendre–Fenchel transform first.

Definition 2.1. ([18, Legendre–Fenchel transform]) For any function $h : \mathcal{X} \rightarrow (-\infty, +\infty]$, function $h^* : \mathcal{X} \rightarrow (-\infty, +\infty]$ defined by

$$(2.1) \quad h^*(\mathbf{w}) := \sup_{\mathbf{f}} \left\{ \langle \mathbf{f}, \mathbf{w} \rangle - h(\mathbf{f}) \right\}$$

is conjugate to h , while function $h^{**} = (h^*)^*$ defined by

$$(2.2) \quad h^{**}(\mathbf{f}) := \sup_{\mathbf{w}} \left\{ \langle \mathbf{f}, \mathbf{w} \rangle - h^*(\mathbf{w}) \right\}$$

is biconjugate to h . The mapping $h \mapsto h^*$ is Legendre–Fenchel transform.

Note that for proper, lower semicontinuous (l.s.c.), convex function, its biconjugate function equals to itself, i.e., $h^{**}(\mathbf{f}) = h(\mathbf{f})$. Moreover, we have the following significant results.

Proposition 2.2. ([18, Inversion rule for subgradient relations]) *For any proper, l.s.c., convex function h , one has $\partial h^* = (\partial h)^{-1}$ and $\partial h = (\partial h^*)^{-1}$. Moreover, if h is Fréchet differentiable, we have $\bar{\mathbf{f}}_h(\mathbf{w}) = \nabla h^*(\mathbf{w})$ and $\bar{\mathbf{w}}_h(\mathbf{f}) = \nabla h(\mathbf{f})$, where $\bar{\mathbf{f}}_h$ and $\bar{\mathbf{w}}_h$ are the optimal solutions to the right-hand sides in (2.1) and (2.2), respectively.*

Subsequently, we introduce proximal mapping and its firm nonexpansivity property, which would be useful for the later convergence analysis.

Definition 2.3. ([3, Proximal mapping]) *Given function $h : \mathcal{X} \rightarrow (-\infty, +\infty]$, the proximal mapping of h is an operator given by*

$$\text{Prox}_h(\mathbf{x}) := \arg \min_{\mathbf{y}} \left\{ h(\mathbf{y}) + \frac{1}{2} \|\mathbf{y} - \mathbf{x}\|^2 \right\}$$

for any $\mathbf{x} \in \mathcal{X}$.

Remark 2.4. Let $\tau > 0$. If h is proper, convex and l.s.c., then $\text{Prox}_{\tau h}(\mathbf{x})$ exists uniquely. Moreover, it is equivalent to the resolvent of subgradient, which is

$$(2.3) \quad \text{Prox}_{\tau h}(\mathbf{x}) = (\text{Id} + \tau \partial h)^{-1}(\mathbf{x}),$$

where Id denotes identity operator (matrix) of the associated vector space.

Proposition 2.5. ([3, Firm nonexpansivity of the proximal operator]) *Let h be a proper closed and convex function. Then, for and $\mathbf{x}, \mathbf{y} \in \mathcal{X}$,*

$$\begin{aligned} \|\text{Prox}_h(\mathbf{x}) - \text{Prox}_h(\mathbf{y})\|^2 &\leq \langle \mathbf{x} - \mathbf{y}, \text{Prox}_h(\mathbf{x}) - \text{Prox}_h(\mathbf{y}) \rangle, \\ \|\text{Prox}_h(\mathbf{x}) - \text{Prox}_h(\mathbf{y})\| &\leq \|\mathbf{x} - \mathbf{y}\|. \end{aligned}$$

3. The proposed extended primal-dual algorithm framework. In this section, we propose a framework of extended primal-dual algorithm for the nonconvex problems in (1.8), where each component K_j of \mathbf{K} is a proper Fréchet differentiable nonlinear convex function in \mathcal{X} .

3.1. The algorithm framework and generated schemes. Let $\bar{\mathbb{R}}_+ := [0, +\infty]$. Assume that $G : \mathcal{X} \rightarrow \bar{\mathbb{R}}_+$, $F^* : \mathcal{Y}_K \rightarrow \bar{\mathbb{R}}_+$ and $E^* : \mathcal{Y}_A \rightarrow \bar{\mathbb{R}}_+$ are proper, convex, l.s.c. functions, and F^* , E^* are themselves the convex conjugates of convex l.s.c. functions F , E , respectively. By Legendre–Fenchel transform in Definition 2.1, the general problem in (1.8) can be translated into the following saddle-point problem

$$(3.1) \quad \min_{\mathbf{f} \in \mathcal{X}} \max_{\mathbf{u} \in \mathcal{Y}_K, \mathbf{v} \in \mathcal{Y}_A} \left\{ \langle \mathbf{K}(\mathbf{f}), \mathbf{u} \rangle + \langle A\mathbf{f}, \mathbf{v} \rangle - F^*(\mathbf{u}) - E^*(\mathbf{v}) + G(\mathbf{f}) \right\},$$

where \mathbf{u} and \mathbf{v} are dual variables regarding the nonlinear and linear operators, respectively.

With the convexity of K_j , by [Definition 2.1](#) again, we obtain

$$(3.2) \quad K_j(\mathbf{f}) = \max_{\mathbf{w}_j} \left\{ \langle \mathbf{f}, \mathbf{w}_j \rangle - K_j^*(\mathbf{w}_j) \right\},$$

where K_j^* is the convex conjugate of K_j . Let $\bar{\mathbf{w}}_j(\mathbf{f})$ be the optimal solution of (3.2). Then, (3.1) becomes

$$(3.3) \quad \min_{\mathbf{f} \in \mathcal{X}} \max_{\mathbf{u} \in \mathcal{Y}_K, \mathbf{v} \in \mathcal{Y}_A} \Phi(\mathbf{f}, \bar{\mathbf{w}}(\mathbf{f}), \mathbf{u}, \mathbf{v}),$$

where

$$\Phi(\mathbf{f}, \bar{\mathbf{w}}(\mathbf{f}), \mathbf{u}, \mathbf{v}) := \sum_j u_j \left\{ \langle \mathbf{f}, \bar{\mathbf{w}}_j(\mathbf{f}) \rangle - K_j^*(\bar{\mathbf{w}}_j(\mathbf{f})) \right\} + \langle A\mathbf{f}, \mathbf{v} \rangle - F^*(\mathbf{u}) - E^*(\mathbf{v}) + G(\mathbf{f}),$$

and $\bar{\mathbf{w}} = [\bar{\mathbf{w}}_1, \dots, \bar{\mathbf{w}}_J]$. Notice that there are many variables in (3.3), which is difficult to solve simultaneously. Thus, it is natural to fix some variables and alternatively solve the associated subproblems. Particularly, we need to update \mathbf{f} and $\bar{\mathbf{w}}(\mathbf{f})$ alternatively for the existing nonlinearity. The proposed framework of extended primal-dual algorithm is presented as the following [Algorithm 3.1](#).

Algorithm 3.1 The proposed extended primal-dual algorithm framework

- 1: *Initialize*: Given $\tau > 0$, $\sigma_K > 0$, $\sigma_A > 0$, $\theta \in [0, 1]$, and initial point $(\mathbf{f}^0, \bar{\mathbf{w}}^0, \mathbf{u}^0, \mathbf{v}^0)$ with $\bar{\mathbf{w}}^0 = \bar{\mathbf{w}}(\mathbf{f}^0)$. Let $\mathbf{f}_\theta^0 \leftarrow \mathbf{f}^0$ and $n \leftarrow 0$.
- 2: *Loop*: Update $(\mathbf{f}^{n+1}, \bar{\mathbf{w}}^{n+1}, \mathbf{u}^{n+1}, \mathbf{v}^{n+1})$ by

$$(3.4a) \quad \mathbf{f}^{n+1} = \arg \min_{\mathbf{f} \in \mathcal{X}} \left\{ \Phi(\mathbf{f}, \bar{\mathbf{w}}^n, \mathbf{u}^n, \mathbf{v}^n) + \frac{1}{2\tau} \|\mathbf{f} - \mathbf{f}^n\|^2 \right\},$$

$$(3.4b) \quad \mathbf{f}_\theta^{n+1} = \mathbf{f}^{n+1} + \theta(\mathbf{f}^{n+1} - \mathbf{f}^n),$$

$$(3.4c) \quad \bar{\mathbf{w}}^{n+1} = \bar{\mathbf{w}}(\bar{\mathbf{f}}^{n+1}) \quad \text{with } \bar{\mathbf{f}}^{n+1} = \mathbf{f}_\theta^{n+1}, \mathbf{f}^{n+1} \text{ or } \mathbf{f}^n,$$

$$(3.4d) \quad \mathbf{u}^{n+1} = \arg \min_{\mathbf{u} \in \mathcal{Y}_K} \left\{ -\Phi(\mathbf{f}_\theta^{n+1}, \bar{\mathbf{w}}^{n+1}, \mathbf{u}, \mathbf{v}^n) + \frac{1}{2\sigma_K} \|\mathbf{u} - \mathbf{u}^n\|^2 \right\},$$

$$(3.4e) \quad \mathbf{v}^{n+1} = \arg \min_{\mathbf{v} \in \mathcal{Y}_A} \left\{ -\Phi(\mathbf{f}_\theta^{n+1}, \bar{\mathbf{w}}^{n+1}, \mathbf{u}^{n+1}, \mathbf{v}) + \frac{1}{2\sigma_A} \|\mathbf{v} - \mathbf{v}^n\|^2 \right\},$$

$$(3.4f) \quad \bar{\mathbf{w}}^{n+1} = \bar{\mathbf{w}}(\tilde{\mathbf{f}}^{n+1}) \quad \text{with } \tilde{\mathbf{f}}^{n+1} = \mathbf{f}_\theta^{n+1} \text{ or } \mathbf{f}^{n+1}.$$

If some given termination condition is satisfied, then **output** \mathbf{f}^{n+1} ; otherwise, let $n \leftarrow n+1$, **goto** *Loop*.

Note that one can update variable $\bar{\mathbf{w}}$ by different ways, which is subsequently generated different extended primal-dual schemes. If the updates in (3.4c) and (3.4f) are the same, we just keep (3.4c).

Before studying more details in [Algorithm 3.1](#), we present a useful result by the following theorem.

Theorem 3.1. *For any proper Fréchet differentiable convex function $h(\mathbf{f})$, suppose $\bar{\mathbf{w}}_h(\mathbf{f}')$ is the optimal solution in the right side of (2.2) corresponding to point \mathbf{f}' . Then*

$$(3.5) \quad \langle \mathbf{f}, \bar{\mathbf{w}}_h(\mathbf{f}') \rangle - h^*(\bar{\mathbf{w}}_h(\mathbf{f}')) = h(\mathbf{f}') + \nabla h(\mathbf{f}')(\mathbf{f} - \mathbf{f}').$$

Proof. Since $\bar{\mathbf{w}}_h(\mathbf{f}')$ is the optimal solution in the right side of (2.2) at \mathbf{f}' , by Proposition 2.2, we obtain $\bar{\mathbf{w}}_h(\mathbf{f}') = \nabla h(\mathbf{f}')$. Taking $\bar{\mathbf{w}}_h(\mathbf{f}')$ into (2.1), then for the optimal solution $\bar{\mathbf{f}}_h(\bar{\mathbf{w}}_h(\mathbf{f}'))$ in the right side of (2.1), by Proposition 2.2 again, we obtain

$$\bar{\mathbf{f}}_h(\bar{\mathbf{w}}_h(\mathbf{f}')) = \nabla h^*(\bar{\mathbf{w}}_h(\mathbf{f}')) = \nabla h^*(\nabla h(\mathbf{f}')) = \mathbf{f}'.$$

Then, by (2.1), and substituting the above equations into the left side of (3.5) yields its right side. \blacksquare

Specifically, using Theorem 3.1, and taking $h(\mathbf{f}) = K_j(\mathbf{f})$, and accordingly $\bar{\mathbf{w}}_h(\mathbf{f}') = \bar{\mathbf{w}}_j(\mathbf{f}')$, we obtain

$$(3.6) \quad \langle \mathbf{f}, \bar{\mathbf{w}}_j(\mathbf{f}') \rangle - K_j^*(\bar{\mathbf{w}}_j(\mathbf{f}')) = K_j(\mathbf{f}') + \nabla K_j(\mathbf{f}')(\mathbf{f} - \mathbf{f}').$$

By (3.3), using (2.3) and (3.6), the update in (3.4a) can be written as

$$\begin{aligned} \mathbf{f}^{n+1} &= \arg \min_{\mathbf{f} \in \mathcal{X}} \left\{ \sum_j u_j^n \left\{ \langle \mathbf{f}, \bar{\mathbf{w}}_j(\bar{\mathbf{f}}^n) \rangle - K_j^*(\bar{\mathbf{w}}_j(\bar{\mathbf{f}}^n)) \right\} + \langle A\mathbf{f}, \mathbf{v}^n \rangle + G(\mathbf{f}) + \frac{1}{2\tau} \|\mathbf{f} - \mathbf{f}^n\|^2 \right\} \\ &\stackrel{(3.6)}{=} \arg \min_{\mathbf{f} \in \mathcal{X}} \left\{ \sum_j u_j^n \nabla K_j(\bar{\mathbf{f}}^n) \mathbf{f} + G(\mathbf{f}) + A^\top \mathbf{v}^n + \frac{1}{2\tau} \|\mathbf{f} - \mathbf{f}^n\|^2 \right\} \\ &\stackrel{(2.3)}{=} (\text{Id} + \tau \partial G)^{-1} \left(\mathbf{f}^n - \tau [\nabla \mathbf{K}(\bar{\mathbf{f}}^n)]^\top \mathbf{u}^n - \tau A^\top \mathbf{v}^n \right). \end{aligned}$$

Similarly, the update in (3.4d) becomes

$$\begin{aligned} \mathbf{u}^{n+1} &= \arg \min_{\mathbf{u} \in \mathcal{Y}_K} \left\{ - \sum_j u_j \left\{ \langle \mathbf{f}_\theta^{n+1}, \bar{\mathbf{w}}_j(\bar{\mathbf{f}}^{n+1}) \rangle - K_j^*(\bar{\mathbf{w}}_j(\bar{\mathbf{f}}^{n+1})) \right\} + F^*(\mathbf{u}) + \frac{1}{2\sigma_K} \|\mathbf{u} - \mathbf{u}^n\|^2 \right\} \\ &\stackrel{(3.6)}{=} \arg \min_{\mathbf{u} \in \mathcal{Y}_K} \left\{ - \langle \mathbf{K}(\bar{\mathbf{f}}^{n+1}) + \nabla \mathbf{K}(\bar{\mathbf{f}}^{n+1})(\mathbf{f}_\theta^{n+1} - \bar{\mathbf{f}}^{n+1}), \mathbf{u} \rangle + F^*(\mathbf{u}) + \frac{1}{2\sigma_K} \|\mathbf{u} - \mathbf{u}^n\|^2 \right\} \\ &\stackrel{(2.3)}{=} (\text{Id} + \sigma_K \partial F^*)^{-1} \left(\mathbf{u}^n + \sigma_K [\mathbf{K}(\bar{\mathbf{f}}^{n+1}) + \nabla \mathbf{K}(\bar{\mathbf{f}}^{n+1})(\mathbf{f}_\theta^{n+1} - \bar{\mathbf{f}}^{n+1})] \right). \end{aligned}$$

Moreover, we have the update in (3.4e) as

$$\begin{aligned} \mathbf{v}^{n+1} &= \arg \min_{\mathbf{v} \in \mathcal{Y}_A} \left\{ - \langle A\mathbf{f}_\theta^{n+1}, \mathbf{v} \rangle + E^*(\mathbf{v}) + \frac{1}{2\sigma_A} \|\mathbf{v} - \mathbf{v}^n\|^2 \right\} \\ &\stackrel{(2.3)}{=} (\text{Id} + \sigma_A \partial E^*)^{-1} (\mathbf{v}^n + \sigma_A A \mathbf{f}_\theta^{n+1}). \end{aligned}$$

Next, we give compact forms of the specific schemes which are generated by updating (3.4c) and (3.4f) in different ways.

I. Let $\bar{f}^{n+1} = f_\theta^{n+1}$ in (3.4c) and $\tilde{f}^{n+1} = f_\theta^{n+1}$ in (3.4f). Then Algorithm 3.1 reduces to the following scheme. We call it EPD-Exact algorithm.

$$(3.7a) \quad f^{n+1} = (\text{Id} + \tau \partial G)^{-1} (f^n - \tau [\nabla K(f_\theta^n)]^\top u^n - \tau A^\top v^n),$$

$$(3.7b) \quad f_\theta^{n+1} = f^{n+1} + \theta (f^{n+1} - f^n),$$

$$(3.7c) \quad u^{n+1} = (\text{Id} + \sigma_K \partial F^*)^{-1} (u^n + \sigma_K K(f_\theta^{n+1})),$$

$$(3.7d) \quad v^{n+1} = (\text{Id} + \sigma_A \partial E^*)^{-1} (v^n + \sigma_A A f_\theta^{n+1}).$$

II. Let $\bar{f}^{n+1} = f^{n+1}$ in (3.4c) and $\tilde{f}^{n+1} = f^{n+1}$ in (3.4f). Then Algorithm 3.1 becomes the following compact scheme, called EPD-Linearized algorithm.

$$(3.8a) \quad f^{n+1} = (\text{Id} + \tau \partial G)^{-1} (f^n - \tau [\nabla K(f^n)]^\top u^n - \tau A^\top v^n),$$

$$(3.8b) \quad f_\theta^{n+1} = f^{n+1} + \theta (f^{n+1} - f^n),$$

$$(3.8c) \quad u^{n+1} = (\text{Id} + \sigma_K \partial F^*)^{-1} (u^n + \sigma_K [K(f^{n+1}) + \nabla K(f^{n+1})(f_\theta^{n+1} - f^{n+1})]),$$

$$(3.8d) \quad v^{n+1} = (\text{Id} + \sigma_A \partial E^*)^{-1} (v^n + \sigma_A A f_\theta^{n+1}).$$

III. Let $\bar{f}^{n+1} = f_\theta^{n+1}$ in (3.4c) and $\tilde{f}^{n+1} = f^{n+1}$ in (3.4f). Then we get

$$(3.9a) \quad f^{n+1} = (\text{Id} + \tau \partial G)^{-1} (f^n - \tau [\nabla K(f^n)]^\top u^n - \tau A^\top v^n),$$

$$(3.9b) \quad f_\theta^{n+1} = f^{n+1} + \theta (f^{n+1} - f^n),$$

$$(3.9c) \quad u^{n+1} = (\text{Id} + \sigma_K \partial F^*)^{-1} (u^n + \sigma_K K(f_\theta^{n+1})),$$

$$(3.9d) \quad v^{n+1} = (\text{Id} + \sigma_A \partial E^*)^{-1} (v^n + \sigma_A A f_\theta^{n+1}).$$

IV. Let $\bar{f}^{n+1} = f^n$ in (3.4c) and $\tilde{f}^{n+1} = f^{n+1}$ in (3.4f). The resulting iterative scheme is

$$(3.10a) \quad f^{n+1} = (\text{Id} + \tau \partial G)^{-1} (f^n - \tau [\nabla K(f^n)]^\top u^n - \tau A^\top v^n),$$

$$(3.10b) \quad f_\theta^{n+1} = f^{n+1} + \theta (f^{n+1} - f^n),$$

$$(3.10c) \quad u^{n+1} = (\text{Id} + \sigma_K \partial F^*)^{-1} (u^n + \sigma_K [K(f^n) + \nabla K(f^n)(f_\theta^{n+1} - f^n)]),$$

$$(3.10d) \quad v^{n+1} = (\text{Id} + \sigma_A \partial E^*)^{-1} (v^n + \sigma_A A f_\theta^{n+1}).$$

Furthermore, we have two more extensions.

V. Let $\bar{f}^{n+1} = f^{n+1}$ in (3.4c) and $\tilde{f}^{n+1} = f_\theta^{n+1}$ in (3.4f). The associated compact form is translated into

$$(3.11a) \quad f^{n+1} = (\text{Id} + \tau \partial G)^{-1} (f^n - \tau [\nabla K(f_\theta^n)]^\top u^n - \tau A^\top v^n),$$

$$(3.11b) \quad f_\theta^{n+1} = f^{n+1} + \theta (f^{n+1} - f^n),$$

$$(3.11c) \quad u^{n+1} = (\text{Id} + \sigma_K \partial F^*)^{-1} (u^n + \sigma_K [K(f^{n+1}) + \nabla K(f^{n+1})(f_\theta^{n+1} - f^{n+1})]),$$

$$(3.11d) \quad v^{n+1} = (\text{Id} + \sigma_A \partial E^*)^{-1} (v^n + \sigma_A A f_\theta^{n+1}).$$

VI. Let $\tilde{f}^{n+1} = f^n$ in (3.4c) and $\tilde{f}^{n+1} = f_\theta^{n+1}$ in (3.4f). The generated iterative scheme is formulated as

$$(3.12a) \quad f^{n+1} = (\text{Id} + \tau \partial G)^{-1} \left(f^n - \tau [\nabla \mathbf{K}(f_\theta^n)]^\top \mathbf{u}^n - \tau A^\top \mathbf{v}^n \right),$$

$$(3.12b) \quad f_\theta^{n+1} = f^{n+1} + \theta (f^{n+1} - f^n),$$

$$(3.12c) \quad \mathbf{u}^{n+1} = (\text{Id} + \sigma_K \partial F^*)^{-1} (\mathbf{u}^n + \sigma_K [\mathbf{K}(f^n) + \nabla \mathbf{K}(f^n)(f_\theta^{n+1} - f^n)]),$$

$$(3.12d) \quad \mathbf{v}^{n+1} = (\text{Id} + \sigma_A \partial E^*)^{-1} (\mathbf{v}^n + \sigma_A A f_\theta^{n+1}).$$

3.2. Relationship to existing algorithms. In this section, we will establish the relationship between the proposed algorithm framework and existing algorithms.

Primal-dual algorithm for convex problem. If \mathbf{K} becomes linear, we execute the above derivation again, and it is easy to validate that the above framework and generated schemes are reduced to the primal-dual algorithm for the convex problem as in (1.9) (or Chambolle–Pock algorithm in [4]). More precisely, we let $\mathbf{K}(f) = \mathbf{K}f$ in this paragraph, then $\nabla \mathbf{K}(f) = \mathbf{K}$, and $\widehat{\Phi}(f, \bar{\mathbf{w}}(f), \mathbf{u}, \mathbf{v})$ is rewritten as

$$\widehat{\Phi}(f, \mathbf{u}, \mathbf{v}) := \langle \mathbf{K}f, \mathbf{u} \rangle + \langle A f, \mathbf{v} \rangle - F^*(\mathbf{u}) - E^*(\mathbf{v}) + G(f).$$

Algorithm 3.1 can be reformulated as the following Algorithm 3.2.

Algorithm 3.2 The primal-dual algorithm for convex problem

1: *Initialize:* Given $\tau > 0$, $\sigma_K > 0$, $\sigma_A > 0$, $\theta \in [0, 1]$, and initial point $(f^0, \mathbf{u}^0, \mathbf{v}^0)$. Let $n \leftarrow 0$.

2: *Loop:* Update $(f^{n+1}, \mathbf{u}^{n+1}, \mathbf{v}^{n+1})$ by

$$(3.13a) \quad f^{n+1} = \arg \min_{f \in \mathcal{X}} \left\{ \widehat{\Phi}(f, \mathbf{u}^n, \mathbf{v}^n) + \frac{1}{2\tau} \|f - f^n\|^2 \right\},$$

$$(3.13b) \quad f_\theta^{n+1} = f^{n+1} + \theta (f^{n+1} - f^n),$$

$$(3.13c) \quad \mathbf{u}^{n+1} = \arg \min_{\mathbf{u} \in \mathcal{Y}_K} \left\{ -\widehat{\Phi}(f_\theta^{n+1}, \mathbf{u}, \mathbf{v}^n) + \frac{1}{2\sigma_K} \|\mathbf{u} - \mathbf{u}^n\|^2 \right\},$$

$$(3.13d) \quad \mathbf{v}^{n+1} = \arg \min_{\mathbf{v} \in \mathcal{Y}_A} \left\{ -\widehat{\Phi}(f_\theta^{n+1}, \mathbf{u}^{n+1}, \mathbf{v}) + \frac{1}{2\sigma_A} \|\mathbf{v} - \mathbf{v}^n\|^2 \right\}.$$

If some given termination condition is satisfied, then **output** f^{n+1} ; otherwise, let $n \leftarrow n+1$, **goto** *Loop*.

Then, all of the generated schemes I–VI are translated into the following unique one.

$$(3.14a) \quad f^{n+1} = (\text{Id} + \tau \partial G)^{-1} (f^n - \tau \mathbf{K}^\top \mathbf{u}^n - \tau A^\top \mathbf{v}^n),$$

$$(3.14b) \quad f_\theta^{n+1} = f^{n+1} + \theta (f^{n+1} - f^n),$$

$$(3.14c) \quad \mathbf{u}^{n+1} = (\text{Id} + \sigma_K \partial F^*)^{-1} (\mathbf{u}^n + \sigma_K \mathbf{K} f_\theta^{n+1}),$$

$$(3.14d) \quad \mathbf{v}^{n+1} = (\text{Id} + \sigma_A \partial E^*)^{-1} (\mathbf{v}^n + \sigma_A A f_\theta^{n+1}).$$

Hence, the proposed algorithm framework can be seen as an extension of the primal-dual algorithm for convex problem.

Exact/Linearized nonlinear PDHGM. It is easy to observe that the exact and linearized nonlinear PDHGM (i.e., Exact NL-PDHGM and Linearized NL-PDHGM) in [20] correspond to schemes (3.9) and (3.10) respectively. It means that we have incorporated these two NL-PDHGM schemes into the proposed algorithm framework. By (3.5) in Theorem 3.1, we establish the relationship between the biconjugate formula and the first-order Taylor expansion of the convex function itself. Equivalently, we provide the complete mathematical explanation for the two iterative schemes, which is easier to understand than the way by using the first-order Taylor expansion as the linear approximation in [20].

Furthermore, the proposed algorithm framework contains more iterative schemes other than the two above, which provides more alternatives to solve the nonconvex optimization problem in (1.8).

Nonconvex primal-dual algorithm. A nonconvex primal-dual algorithm, namely, nonconvex Chambolle–Pock algorithm, is proposed to solve the image reconstruction model in spectral CT with various convex functionals including total variation (TV) norm as constraint rather than regularization term [6, 7], but which can be also extended as an alternative to solving the model (1.8). Here we do not state that algorithm itself in detail, but just focus on the way to linearize the nonlinear $\mathbf{K}(\mathbf{f})$ at related step.

In [7, eq. (10)] or [6, Algorithm 2], $\mathbf{K}(\mathbf{f})$ is linearized at current point \mathbf{f}^n equivalently by

$$(3.15) \quad \mathbf{K}(\mathbf{f}) \approx \mathbf{K}(\mathbf{f}^n) + \nabla \mathbf{K}(0)(\mathbf{f} - \mathbf{f}^n),$$

where $\nabla \mathbf{K}(0)$ is definitely the constant matrix \mathcal{H} in that algorithm. Thus, in what follows we can obtain the corresponding general iterative scheme as

$$(3.16a) \quad \mathbf{f}^{n+1} = (\text{Id} + \tau \partial G)^{-1} \left(\mathbf{f}^n - \tau [\nabla \mathbf{K}(0)]^\top \mathbf{u}^n - \tau A^\top \mathbf{v}^n \right),$$

$$(3.16b) \quad \mathbf{f}_\theta^{n+1} = \mathbf{f}^{n+1} + \theta (\mathbf{f}^{n+1} - \mathbf{f}^n),$$

$$(3.16c) \quad \mathbf{u}^{n+1} = (\text{Id} + \sigma_K \partial F^*)^{-1} (\mathbf{u}^n + \sigma_K [\mathbf{K}(\mathbf{f}^n) + \nabla \mathbf{K}(0)(\mathbf{f}_\theta^{n+1} - \mathbf{f}^n)]),$$

$$(3.16d) \quad \mathbf{v}^{n+1} = (\text{Id} + \sigma_A \partial E^*)^{-1} (\mathbf{v}^n + \sigma_A A \mathbf{f}_\theta^{n+1}).$$

Remark that the linearization in (3.15) is not exactly the first-order Taylor expansion of $\mathbf{K}(\mathbf{f})$ at \mathbf{f}^n , which applies $\nabla \mathbf{K}(0)$ instead of gradient $\nabla \mathbf{K}(\mathbf{f}^n)$. The accuracy of the linear approximation in (3.15) is only $O(\|\mathbf{f} - \mathbf{f}^n\|)$, which carries with much lower accuracy than $O(\|\mathbf{f} - \mathbf{f}^n\|^2)$ by the first-order Taylor expansion. However, if \mathbf{K} is much close to a linear operator, such approximation would be effective.

Nonconvex ADMM. The authors proposed a nonconvex ADMM in [2, Algorithm 1] to solve the optimization problem as

$$(3.17) \quad \min_{\mathbf{f}, \mathbf{y}} \{F_1(\mathbf{f}) + F_2(\mathbf{y})\}, \quad \text{s.t. } A\mathbf{f} + B\mathbf{y} = \mathbf{c},$$

where F_1 and F_2 are potentially nonconvex and/or nondifferentiable.

As an alternative, we can use the nonconvex ADMM to solve model (1.8) explicitly. To proceed, we need to introduce one auxiliary variable $\mathbf{y} = A\mathbf{f}$, and then model (1.8) can be

rewritten as

$$(3.18) \quad \min_{\mathbf{f}, \mathbf{y}} \left\{ \underbrace{(F \circ \mathbf{K})(\mathbf{f}) + G(\mathbf{f})}_{F_1(\mathbf{f})} + \underbrace{E(\mathbf{y})}_{F_2(\mathbf{y})} \right\}, \quad \text{s.t. } A\mathbf{f} - \mathbf{y} = 0,$$

where assume that $F \circ \mathbf{K}$ is differentiable but nonconvex, and G and E are convex but non-differentiable. Then, the nonconvex ADMM for problem (3.18) is given as the following [Algorithm 3.3](#).

Algorithm 3.3 The nonconvex ADMM for the model in (1.8)

- 1: *Initialize*: Given $\tau > 0$, $\sigma > 0$, initial point $(\mathbf{f}^0, \mathbf{y}^0, \mathbf{z}^0)$, and positive matrices P_0 , P_1 and P_2 . Let $n \leftarrow 0$.
- 2: *Loop*: Update $(\mathbf{f}^{n+1}, \mathbf{y}^{n+1}, \mathbf{z}^{n+1})$ by

$$(3.19a) \quad \mathbf{f}^{n+1} = \arg \min_{\mathbf{f}} \left\{ G(\mathbf{f}) + \langle \mathbf{f}, \nabla(F \circ \mathbf{K})(\mathbf{f}^n) + A^\top \mathbf{z}^n \rangle + \frac{1}{2} \|A\mathbf{f} - \mathbf{y}^n\|_{P_0}^2 + \frac{1}{2\tau} \|\mathbf{f} - \mathbf{f}^n\|_{P_1}^2 \right\},$$

$$(3.19b) \quad \mathbf{y}^{n+1} = \arg \min_{\mathbf{y}} \left\{ E(\mathbf{y}) - \langle \mathbf{y}, \mathbf{z}^n \rangle + \frac{1}{2} \|A\mathbf{f}^{n+1} - \mathbf{y}\|_{P_0}^2 + \frac{1}{2\sigma} \|\mathbf{y} - \mathbf{y}^n\|_{P_2}^2 \right\},$$

$$(3.19c) \quad \mathbf{z}^{n+1} = \mathbf{z}^n + A\mathbf{f}^{n+1} - \mathbf{y}^{n+1}.$$

If some given termination condition is satisfied, then **output** \mathbf{f}^{n+1} ; otherwise, let $n \leftarrow n+1$, **goto** *Loop*.

Note that the auxiliary variables are often required to introduce in order to use nonconvex ADMM. Since $F \circ \mathbf{K}$ is a nonlinear differentiable function, linear approximation also needs to be used directly and taken as its first-order Taylor expansion at current point \mathbf{f}^n in (3.19a). Moreover, the inner iteration is probably required to solve the subproblem in (3.19a) for the existence of A in the third term of the objective function.

4. Convergence analysis. Without loss of generality, we mainly present the convergence analysis for iterative schemes (3.7) and (3.8). For ease of analyzing algorithm convergence, we take acceleration parameter $\theta = 1$ in [Algorithm 3.1](#). We assume that problem (3.1) has at least one solution $\widehat{\boldsymbol{\beta}} := [\widehat{\mathbf{f}}^\top, \widehat{\mathbf{u}}^\top, \widehat{\mathbf{v}}^\top]^\top$ such that

$$(4.1) \quad 0 \in H(\widehat{\boldsymbol{\beta}}) := \begin{bmatrix} \partial G(\widehat{\mathbf{f}}) + [\nabla \mathbf{K}(\widehat{\mathbf{f}})]^\top \widehat{\mathbf{u}} + A^\top \widehat{\mathbf{v}} \\ \partial F^*(\widehat{\mathbf{u}}) - \mathbf{K}(\widehat{\mathbf{f}}) \\ \partial E^*(\widehat{\mathbf{v}}) - A\widehat{\mathbf{f}} \end{bmatrix}.$$

By the definition and property of proximal mapping, we can rewrite the updates in (3.7) as

$$(4.2) \quad 0 \in \begin{bmatrix} \partial G(\mathbf{f}_\theta^{n+1}) + [\nabla \mathbf{K}(\mathbf{f}_\theta^n)]^\top \mathbf{u}^n + A^\top \mathbf{v}^n + \tau^{-1}(\mathbf{f}^{n+1} - \mathbf{f}^n) \\ \partial F^*(\mathbf{u}^{n+1}) - \mathbf{K}(\mathbf{f}_\theta^{n+1}) + \sigma_K^{-1}(\mathbf{u}^{n+1} - \mathbf{u}^n) \\ \partial E^*(\mathbf{v}^{n+1}) - A\mathbf{f}_\theta^{n+1} + \sigma_A^{-1}(\mathbf{v}^{n+1} - \mathbf{v}^n) \end{bmatrix},$$

and the updates in (3.8) as

$$(4.3) \quad 0 \in \begin{bmatrix} \partial G(\mathbf{f}^{n+1}) + [\nabla \mathbf{K}(\mathbf{f}^n)]^\top \mathbf{u}^n + A^\top \mathbf{v}^n + \tau^{-1}(\mathbf{f}^{n+1} - \mathbf{f}^n) \\ \partial F^*(\mathbf{u}^{n+1}) - \mathbf{K}(\mathbf{f}^{n+1}) - \nabla \mathbf{K}(\mathbf{f}^{n+1})(\mathbf{f}_\theta^{n+1} - \mathbf{f}^{n+1}) + \sigma_K^{-1}(\mathbf{u}^{n+1} - \mathbf{u}^n) \\ \partial E^*(\mathbf{v}^{n+1}) - A\mathbf{f}_\theta^{n+1} + \sigma_A^{-1}(\mathbf{v}^{n+1} - \mathbf{v}^n) \end{bmatrix}.$$

Let $\boldsymbol{\beta}^n := [\mathbf{f}^{n\top}, \mathbf{u}^{n\top}, \mathbf{v}^{n\top}]^\top$ and

$$(4.4) \quad M(\mathbf{f}) := \begin{bmatrix} \tau^{-1} \text{Id} & -[\nabla \mathbf{K}(\mathbf{f})]^\top & -A^\top \\ -\nabla \mathbf{K}(\mathbf{f}) & \sigma_K^{-1} \text{Id} & 0 \\ -A & 0 & \sigma_A^{-1} \text{Id} \end{bmatrix}.$$

Then we respectively simplify the above update formulas in (4.2) and (4.3) as

$$(4.5) \quad 0 \in \tilde{H}_{n+1}^1(\boldsymbol{\beta}^{n+1}) + M_{n+1}^1(\boldsymbol{\beta}^{n+1} - \boldsymbol{\beta}^n)$$

and

$$(4.6) \quad 0 \in \tilde{H}_{n+1}^2(\boldsymbol{\beta}^{n+1}) + M_{n+1}^2(\boldsymbol{\beta}^{n+1} - \boldsymbol{\beta}^n),$$

where $M_{n+1}^1 := M(\mathbf{f}_\theta^n)$, $M_{n+1}^2 := M(\mathbf{f}^n)$,

$$\tilde{H}_{n+1}^1(\boldsymbol{\beta}^{n+1}) := \begin{bmatrix} \partial G(\mathbf{f}^{n+1}) + [\nabla \mathbf{K}(\mathbf{f}_\theta^n)]^\top \mathbf{u}^{n+1} + A^\top \mathbf{v}^{n+1} \\ \partial F^*(\mathbf{u}^{n+1}) - \mathbf{K}(\mathbf{f}_\theta^{n+1}) + \nabla \mathbf{K}(\mathbf{f}_\theta^n)(\mathbf{f}^{n+1} - \mathbf{f}^n) \\ \partial E^*(\mathbf{v}^{n+1}) - A\mathbf{f}_\theta^{n+1} + A(\mathbf{f}^{n+1} - \mathbf{f}^n) \end{bmatrix},$$

and

$$\tilde{H}_{n+1}^2(\boldsymbol{\beta}^{n+1}) := \begin{bmatrix} \partial G(\mathbf{f}^{n+1}) + [\nabla \mathbf{K}(\mathbf{f}^n)]^\top \mathbf{u}^{n+1} + A^\top \mathbf{v}^{n+1} \\ \partial F^*(\mathbf{u}^{n+1}) - \mathbf{K}(\mathbf{f}^{n+1}) - \nabla \mathbf{K}(\mathbf{f}^{n+1})(\mathbf{f}_\theta^{n+1} - \mathbf{f}^{n+1}) + \nabla \mathbf{K}(\mathbf{f}^n)(\mathbf{f}^{n+1} - \mathbf{f}^n) \\ \partial E^*(\mathbf{v}^{n+1}) - A\mathbf{f}_\theta^{n+1} + A(\mathbf{f}^{n+1} - \mathbf{f}^n) \end{bmatrix}.$$

Subsequently, as a representative, we just give the convergence analysis for (4.5) and (4.6), which represent schemes (3.7) and (3.8) respectively.

4.1. Basic assumption and result. Here we introduce some local assumptions. Before this, we define a neighborhood of $\hat{\boldsymbol{\beta}}$ as

$$\mathcal{O}(\rho_f, \rho_u, \rho_v) := \mathcal{B}_{\hat{\mathbf{f}}}(\rho_f) \times \mathcal{B}_{\hat{\mathbf{u}}}(\rho_u) \times \mathcal{B}_{\hat{\mathbf{v}}}(\rho_v),$$

where $\mathcal{B}_{\hat{\mathbf{f}}}(r) := \{\mathbf{f} \in \mathcal{X} : \|\mathbf{f} - \hat{\mathbf{f}}\| \leq r\}$, and $\mathcal{B}_{\hat{\mathbf{u}}}(r)$, $\mathcal{B}_{\hat{\mathbf{v}}}(r)$ are defined in the same way.

Assumption 1. (Strongly monotone of ∂F^*) The set-valued mapping ∂F^* is γ_{F^*} -strongly monotone at $\hat{\mathbf{u}}$ in $\mathcal{B}_{\hat{\mathbf{u}}}(\rho_u)$, which holds

$$\langle \partial F^*(\mathbf{u}) - \partial F^*(\hat{\mathbf{u}}), \mathbf{u} - \hat{\mathbf{u}} \rangle \geq \gamma_{F^*} \|\mathbf{u} - \hat{\mathbf{u}}\|^2$$

for any $\mathbf{u} \in \mathcal{B}_{\hat{\mathbf{u}}}(\rho_u)$.

Remark 4.1. Here we only need ∂F^* rather than both ∂F^* and ∂G to be strongly monotone, which implies a weaker assumption than [9, Assumption 3.3].

Assumption 2. (Locally Lipschitz of ∇K) Let $\mathbf{K} : \mathcal{X} \rightarrow \mathcal{Y}_K$ be Fréchet differentiable, and there are some $L \geq 0$ such that

$$(4.7) \quad \|\nabla \mathbf{K}(\mathbf{f}) - \nabla \mathbf{K}(\mathbf{x})\| \leq L\|\mathbf{f} - \mathbf{x}\|$$

for any $\mathbf{f}, \mathbf{x} \in \mathcal{B}_{\widehat{\mathbf{f}}}(\rho_f)$.

In addition, we require a restriction on the nonlinearity of \mathbf{K} .

Assumption 3. (Nonlinearity restriction of \mathbf{K}) Assume that $\widehat{\mathbf{u}} \neq 0$. For any $\mathbf{f}, \mathbf{x} \in \mathcal{B}_{\widehat{\mathbf{f}}}(\rho_f)$, $\mathbf{u} \in \mathcal{B}_{\widehat{\mathbf{u}}}(\rho_u)$, there are some $\gamma_1 \in \mathbb{R}$ and $\lambda_1 \geq 0$, such that

$$\begin{aligned} \langle [\nabla \mathbf{K}(\mathbf{x}) - \nabla \mathbf{K}(\widehat{\mathbf{f}})](\mathbf{f} - \widehat{\mathbf{f}}), \widehat{\mathbf{u}} \rangle + \langle \mathbf{K}(\widehat{\mathbf{f}}) - \mathbf{K}(\mathbf{f}) - \nabla \mathbf{K}(\mathbf{f})(\widehat{\mathbf{f}} - \mathbf{f}), \mathbf{u} - \widehat{\mathbf{u}} \rangle \\ \geq -\gamma_1 \|\mathbf{u} - \widehat{\mathbf{u}}\|^2 - \lambda_1 \|\mathbf{f} - \mathbf{x}\|^2. \end{aligned}$$

Remark 4.2. If \mathbf{K} is linear, the above inequality holds explicitly for any $\gamma_1 \geq 0$ and $\lambda_1 \geq 0$. In fact, Assumption 3 restricts operator \mathbf{K} not too far from linear operator, in other words, whose second-order remainder is sufficiently small.

Remark 4.3. If $\widehat{\mathbf{u}} = 0$, for any $\mathbf{x} = \mathbf{f} \in \mathcal{B}_{\widehat{\mathbf{f}}}(\rho_f)$, we have

$$\langle \mathbf{K}(\widehat{\mathbf{f}}) - \mathbf{K}(\mathbf{f}) - \nabla \mathbf{K}(\mathbf{f})(\widehat{\mathbf{f}} - \mathbf{f}), \mathbf{u} \rangle \geq -\gamma_1 \|\mathbf{u}\|^2.$$

Now we fix \mathbf{f} and let $\mathbf{u}' = \mathbf{K}(\widehat{\mathbf{f}}) - \mathbf{K}(\mathbf{f}) - \nabla \mathbf{K}(\mathbf{f})(\widehat{\mathbf{f}} - \mathbf{f}) \neq 0$. We can take $\mathbf{u} = c\mathbf{u}'$ for $0 < c < c_1$ so that $\mathbf{u} \in \mathcal{B}_{\widehat{\mathbf{u}}}(\rho_u)$. Substituting them into the above inequality yields $1 \leq \gamma_1 c$. However we can always take c sufficiently small to make this inequality invalid. So this is the reason why we need to restrict $\widehat{\mathbf{u}} \neq 0$ in Assumption 3.

The following theorem in [9] would be useful for our convergence analysis.

Theorem 4.4. ([9]) In a Hilbert space \mathcal{H} , let $M_{n+1} \in \mathcal{L}(\mathcal{H}, \mathcal{H})$, suppose

$$0 \in \widetilde{H}_{n+1}(\boldsymbol{\beta}^{n+1}) + M_{n+1}(\boldsymbol{\beta}^{n+1} - \boldsymbol{\beta}^n)$$

is solvable for iterates $\{\boldsymbol{\beta}^n\}_{n \in \mathbb{N}}$. If M_{n+1} is symmetric positive semidefinite and

$$(4.8) \quad \langle \widetilde{H}_{n+1}(\boldsymbol{\beta}^{n+1}), \boldsymbol{\beta}^{n+1} - \widehat{\boldsymbol{\beta}} \rangle - \frac{1}{2} \|\boldsymbol{\beta}^{n+1} - \widehat{\boldsymbol{\beta}}\|_{M_{n+2}-M_{n+1}}^2 + \frac{1}{2} \|\boldsymbol{\beta}^{n+1} - \boldsymbol{\beta}^n\|_{M_{n+1}}^2 \geq \mathcal{V}_{n+1}$$

for a fixed $n \in \mathbb{N}$, some $\widehat{\boldsymbol{\beta}} \in \mathcal{H}$ and $\mathcal{V}_{n+1} \in \mathbb{R}$, then

$$(4.9) \quad \frac{1}{2} \|\boldsymbol{\beta}^{n+1} - \widehat{\boldsymbol{\beta}}\|_{M_{n+2}}^2 + \mathcal{V}_{n+1} \leq \frac{1}{2} \|\boldsymbol{\beta}^n - \widehat{\boldsymbol{\beta}}\|_{M_{n+1}}^2.$$

Moreover, if (4.9) holds for all $0 \leq n \leq N$ ($N \geq 1$), then we have

$$(4.10) \quad \frac{1}{2} \|\boldsymbol{\beta}^{N+1} - \widehat{\boldsymbol{\beta}}\|_{M_{N+2}}^2 + \sum_{n=0}^N \mathcal{V}_{n+1} \leq \frac{1}{2} \|\boldsymbol{\beta}^0 - \widehat{\boldsymbol{\beta}}\|_{M_1}^2.$$

4.2. Convergence results. Here we present convergence results for the proposed schemes. As we can see, [Theorem 4.4](#) requires that a local metric is constructed by M_{n+1} and the descent estimate inequality [\(4.8\)](#) holds. To this end, we first give the following lemma.

Lemma 4.5. *Let $0 < s, \kappa < 1$, $C_K = \sup_{\mathcal{B}_{\hat{f}}(\rho_f)} \|\nabla K(\mathbf{f})\|$ and*

$$\begin{aligned} B_1(\mathbf{f}) &:= \text{diag}\left(\frac{\kappa}{\tau} \text{Id}, \frac{1}{\sigma_K} \text{Id} - \frac{\tau}{s(1-\kappa)} \nabla K(\mathbf{f}) \nabla K(\mathbf{f})^\top, \frac{1}{\sigma_A} \text{Id} - \frac{\tau}{(1-s)(1-\kappa)} A A^\top\right), \\ B_2(\mathbf{f}) &:= \text{diag}\left(\frac{1}{\tau} \text{Id} - \frac{\sigma_K}{1-\kappa} \nabla K(\mathbf{f})^\top \nabla K(\mathbf{f}) - \frac{\sigma_A}{1-\kappa} A^\top A, \frac{\kappa}{\sigma_K} \text{Id}, \frac{\kappa}{\sigma_A} \text{Id}\right). \end{aligned}$$

Assume that step sizes τ , σ_K , and σ_A satisfy

$$(4.11) \quad \tau \sigma_K C_K^2 < s(1-\kappa), \quad \tau \sigma_A \|A\|^2 < (1-s)(1-\kappa),$$

then $M(\mathbf{f})$ defined in [\(4.4\)](#) is symmetric positive semidefinite such that

$$M(\mathbf{f}) \geq B_1(\mathbf{f}) \geq 0 \quad \text{and} \quad M(\mathbf{f}) \geq B_2(\mathbf{f}) \geq 0$$

for any $\mathbf{f} \in \mathcal{B}_{\hat{f}}(\rho_f)$.

Proof. See [Appendix A.1](#) for the proof. ■

Next, we present the following lemma.

Lemma 4.6. *Assume that $G : \mathcal{X} \rightarrow \overline{\mathbb{R}}_+$, $F^* : \mathcal{Y}_K \rightarrow \overline{\mathbb{R}}_+$ and $E^* : \mathcal{Y}_A \rightarrow \overline{\mathbb{R}}_+$ are proper, convex, l.s.c. functions, and $\mathbf{f}_\theta^{n+1} \in \mathcal{B}_{\hat{f}}(\rho_f)$, $\boldsymbol{\beta}^n, \boldsymbol{\beta}^{n+1} \in \mathcal{O}(\rho_f, \rho_u, \rho_v)$. Moreover, [Assumption 1–Assumption 3](#) and the conditions in [Lemma 4.5](#) hold in $\mathcal{O}(\rho_f, \rho_u, \rho_v)$. Then, we have the following estimate for scheme [\(3.7\)](#)*

$$(4.12) \quad \begin{aligned} \langle \tilde{H}_{n+1}^1(\boldsymbol{\beta}^{n+1}), \boldsymbol{\beta}^{n+1} - \hat{\boldsymbol{\beta}} \rangle - \frac{1}{2} \|\boldsymbol{\beta}^{n+1} - \hat{\boldsymbol{\beta}}\|_{M_{n+2}^1 - M_{n+1}^1}^2 + \frac{1}{2} \|\boldsymbol{\beta}^{n+1} - \boldsymbol{\beta}^n\|_{M_{n+1}^1}^2 \\ \geq (\gamma_{F^*} - \gamma_1 - \tilde{C}) \|\mathbf{u}^{n+1} - \hat{\mathbf{u}}\|^2 + \Lambda_1(\tau) \|\mathbf{f}^{n+1} - \mathbf{f}^n\|^2 \\ - \left(2\lambda_1 + \frac{L\rho_u}{2}\right) \|\mathbf{f}^{n-1} - \mathbf{f}^n\|^2, \end{aligned}$$

where $\tilde{C} := C_K + L\rho_f/2$, $\Lambda_1(\tau) := \kappa/2\tau - (\tilde{C} + 2\lambda_1 + 5L\rho_u/2)$, and the following estimate for scheme [\(3.8\)](#)

$$(4.13) \quad \begin{aligned} \langle \tilde{H}_{n+1}^2(\boldsymbol{\beta}^{n+1}), \boldsymbol{\beta}^{n+1} - \hat{\boldsymbol{\beta}} \rangle - \frac{1}{2} \|\boldsymbol{\beta}^{n+1} - \hat{\boldsymbol{\beta}}\|_{M_{n+2}^2 - M_{n+1}^2}^2 + \frac{1}{2} \|\boldsymbol{\beta}^{n+1} - \boldsymbol{\beta}^n\|_{M_{n+1}^2}^2 \\ \geq (\gamma_{F^*} - \gamma_1) \|\mathbf{u}^{n+1} - \hat{\mathbf{u}}\|^2 + \Lambda_2(\tau) \|\mathbf{f}^{n+1} - \mathbf{f}^n\|^2, \end{aligned}$$

where $\Lambda_2(\tau) := \kappa/2\tau - (\lambda_1 + L\rho_u)$.

Proof. See [Appendix A.2](#) for the proof. ■

Then we have the following corollary.

Corollary 4.7. *Under the assumptions of Lemma 4.6, suppose further that $\gamma_{F^*} > \gamma_1 + \tilde{C}$. If step size τ satisfies*

$$(4.14) \quad \tau < \frac{\kappa}{2(\tilde{C} + 4\lambda_1 + 3L\rho_u)},$$

then $\{\boldsymbol{\beta}^n\}_{n \in \mathbb{N}}$ that generated by scheme (3.7) fulfils

$$(4.15) \quad \|\boldsymbol{\beta}^{n+1} - \widehat{\boldsymbol{\beta}}\|_{M_{n+2}^1} \leq \|\boldsymbol{\beta}^0 - \widehat{\boldsymbol{\beta}}\|_{M_1^1}.$$

Furthermore, if step size τ satisfies

$$(4.16) \quad \tau < \frac{\kappa}{2(\lambda_1 + L\rho_u)},$$

then $\{\boldsymbol{\beta}^n\}_{n \in \mathbb{N}}$ produced by scheme (3.8) have the following relationship

$$(4.17) \quad \|\boldsymbol{\beta}^{n+1} - \widehat{\boldsymbol{\beta}}\|_{M_{n+2}^2} \leq \|\boldsymbol{\beta}^n - \widehat{\boldsymbol{\beta}}\|_{M_{n+1}^2} \leq \dots \leq \|\boldsymbol{\beta}^0 - \widehat{\boldsymbol{\beta}}\|_{M_1^2}.$$

Proof. The proof is referred to Appendix A.3. ■

Moreover, we need to verify that assumptions $\mathbf{f}_\theta^{n+1} \in \mathcal{B}_{\tilde{f}}(\rho_f)$ and $\boldsymbol{\beta}^n, \boldsymbol{\beta}^{n+1} \in \mathcal{O}(\rho_f, \rho_u, \rho_v)$ hold in Lemma 4.6. The case for scheme (3.7) will be proven in the following lemma, and it can be proven for scheme (3.8) by the same method.

Lemma 4.8. *Given $\rho_f, \rho_u, \rho_v > 0$, assume that Assumption 1 with $\gamma_{F^*} > \gamma_1 + \tilde{C}$, and Assumption 2 and Assumption 3 hold, and step sizes τ, σ_K and σ_A satisfy (4.11) and (4.14), and initial point $\boldsymbol{\beta}^0 \in \mathcal{O}(r_f, r_u, r_v)$ such that*

$$(4.18) \quad \|\boldsymbol{\beta}^0 - \widehat{\boldsymbol{\beta}}\|_{M_1^1} \leq \min\{r_f \sqrt{\kappa/\tau}, r_u \sqrt{\kappa/\sigma_K}, r_v \sqrt{\kappa/\sigma_A}\},$$

where $r_f + 2C_f \leq \rho_f$, $r_u + C_u \leq \rho_u$, $r_v + C_v \leq \rho_v$, and

$$C_f := \tau((r_u + 2\|\widehat{\mathbf{u}}\|)C_K + \|A\|r_v), \quad C_u := \sigma_K(r_f + 2C_f)C_K, \quad C_v := \sigma_A(r_f + 2C_f)\|A\|.$$

Then for the iterate sequence generated by scheme (3.7), $\boldsymbol{\beta}^n \in \mathcal{O}(\rho_f, \rho_u, \rho_v)$, and $\mathbf{f}_\theta^{n+1} \in \mathcal{B}_{\tilde{f}}(\rho_f)$ hold for all n .

Proof. See Appendix A.4 for the proof. ■

Finally, we apply the previous analysis to conclude convergent results for the proposed algorithm framework. Here we only give the convergence theorem for scheme (3.7), without loss of generality.

Theorem 4.9. *Assume that $G : \mathcal{X} \rightarrow \overline{\mathbb{R}}_+$, $F^* : \mathcal{Y}_K \rightarrow \overline{\mathbb{R}}_+$ and $E^* : \mathcal{Y}_A \rightarrow \overline{\mathbb{R}}_+$ are proper, convex, l.s.c. functions. Under the conditions in Lemma 4.8, iterate sequence $\{\boldsymbol{\beta}^n\}_{n \in \mathbb{N}}$ generated by scheme (3.7) converges to some point which satisfies the optimal conditions in (4.1).*

Proof. The proof is referred to Appendix A.5. ■

Remark 4.10. Since problem (3.1) may have more than one solutions, Theorem 4.9 only shows that Algorithm 3.1 converges to some point which may not be the solution we assumed previously.

Remark 4.11. Similarly, under the assumptions in subsection 4.1, the convergence of the other schemes can be given. Just some conditions need to be slightly modified, for instance, $\gamma_{F^*} > \gamma_1$ required; the two linearized schemes (3.8) and (3.10) require that (4.16) is satisfied; scheme (3.9) requires $\tau < \kappa/(2\lambda_1 + L\rho_{\mathbf{u}})$. The left proofs of them are analogous.

5. Application to nonlinear imaging. We illustrate the effectiveness of the proposed algorithm framework for nonlinear imaging problems. In this section, we specifically consider the image reconstruction in spectral CT.

To this end, in (1.6), we take the data fidelity term as

$$(5.1) \quad \mathcal{D}(\mathbf{K}(\mathbf{f}), \mathbf{g}) := \frac{1}{2} \|\mathbf{K}(\mathbf{f}) - \mathbf{g}\|_2^2,$$

where the component of $\mathbf{K}(\mathbf{f})$ is defined as (1.2), and the regularization term is given as TV functional [19], i.e.,

$$\mathcal{R}(\mathbf{f}) := \lambda \|\nabla \mathbf{f}\|_1.$$

Here $\nabla = \text{diag}(\nabla_1, \dots, \nabla_D)$ (i.e., the $A := \nabla$ in (1.7)), ∇_d denotes associated discrete form of the gradient operator for \mathbf{f}_d , and $\Omega := \mathbb{R}_+^{DN}$ represents the space of nonnegative vectors. Hence, the specific optimization problem for image reconstruction in spectral CT can be formulated as

$$(5.2) \quad \min_{\mathbf{f} \in \mathbb{R}_+^{DN}} \left\{ \frac{1}{2} \|\mathbf{K}(\mathbf{f}) - \mathbf{g}\|_2^2 + \lambda \|\nabla \mathbf{f}\|_1 \right\}.$$

Note that model (5.2) is actually equivalent to the model that changed the TV regularization term into an inequality constraint, and the latter one has been considered in [7]. For (5.2), the general framework in (1.8) is specified by

$$(5.3) \quad F(\mathbf{K}(\mathbf{f})) := \frac{1}{2} \|\mathbf{K}(\mathbf{f}) - \mathbf{g}\|_2^2,$$

$$(5.4) \quad E(A\mathbf{f}) := \lambda \|\nabla \mathbf{f}\|_1,$$

$$(5.5) \quad G(\mathbf{f}) := \begin{cases} 0 & \text{if } \mathbf{f} \in \mathbb{R}_+^{DN}, \\ +\infty & \text{otherwise.} \end{cases}$$

Accordingly, we derive that

$$(5.6) \quad F^*(\mathbf{u}) = \frac{1}{2} \|\mathbf{u}\|^2 + \langle \mathbf{g}, \mathbf{u} \rangle,$$

$$(5.7) \quad E^*(\mathbf{v}) = \delta_{\text{Box}(\lambda)}(\mathbf{v}) = \begin{cases} 0, & \text{if } \mathbf{v} \in \text{Box}(\lambda) := \{\mathbf{v} : \|\mathbf{v}\|_\infty \leq \lambda\}, \\ +\infty, & \text{otherwise.} \end{cases}$$

It is obvious that here G , F^* and E^* are proper, convex, l.s.c. functions, and F^* is strongly convex. Furthermore, we give some significant results about the \mathbf{K}_j in (1.2) by the following theorem.

Theorem 5.1. *For any given finite sequence $\{b_{dm}\}$ for $1 \leq d \leq D$ and $1 \leq m \leq M$, \mathbf{K}_j defined in (1.2) is Fréchet differentiable and convex with respect to \mathbf{f} . Furthermore, its gradient $\nabla \mathbf{K}_j$ is global Lipschitz continuous.*

Proof. The proof is given in [Appendix A.6](#). ■

As a result, the proposed algorithm framework can be used to solve the image reconstruction problem for spectral CT in (5.2). By [Definition 2.3](#), (2.3) and the definitions of G , F^* and E^* as the above, we have $(\text{Id} + \tau \partial G)^{-1}(\mathbf{f}) = \text{Proj}_{\Omega}(\mathbf{f})$, $(\text{Id} + \sigma_A \partial E^*)^{-1}(\mathbf{v}) = \text{Proj}_{\text{Box}(\lambda)}(\mathbf{v})$ and

$$(\text{Id} + \sigma_K \partial F^*)^{-1}(\mathbf{u}) = \frac{\mathbf{u} - \sigma_K \mathbf{g}}{\sigma_K + 1},$$

where Proj_{Ω} and $\text{Proj}_{\text{Box}(\lambda)}$ denote the orthogonal projection operators onto Ω and $\text{Box}(\lambda)$ respectively. Hence, the proposed scheme in (3.7) can be explicitly written as

$$(5.8a) \quad \mathbf{f}^{n+1} = \text{Proj}_{\Omega} \left(\mathbf{f}^n - \tau [(\nabla \mathbf{K}(\mathbf{f}_{\theta}^n))^{\top} \mathbf{u}^n + \nabla^{\top} \mathbf{v}^n] \right),$$

$$(5.8b) \quad \mathbf{f}_{\theta}^{n+1} = \mathbf{f}^{n+1} + \theta(\mathbf{f}^{n+1} - \mathbf{f}^n),$$

$$(5.8c) \quad \mathbf{u}^{n+1} = \frac{\mathbf{u}^n + \sigma_K (\mathbf{K}(\mathbf{f}_{\theta}^{n+1}) - \mathbf{g})}{\sigma_K + 1},$$

$$(5.8d) \quad \mathbf{v}^{n+1} = \text{Proj}_{\text{Box}(\lambda)}(\mathbf{v}^n + \sigma_A \nabla \mathbf{f}_{\theta}^{n+1}).$$

Similarly, we can easily figure out the other specific schemes using (3.8)–(3.12).

5.1. Convergence analysis for $\hat{\mathbf{u}} = 0$. Note that $\hat{\mathbf{u}}$ is an optimal dual variable which corresponds to the nonlinear operator in problem (3.1). In [section 4](#), we analyzed the convergence of the proposed schemes under the case of $\hat{\mathbf{u}} \neq 0$ as in [Assumption 3](#). Here we further analyze the convergence for the case $\hat{\mathbf{u}} = 0$ specially to scheme (5.8) in spectral CT reconstruction. Recalling the optimal conditions in (4.1), and by (5.6), we have $\hat{\mathbf{u}} + \mathbf{g} - \mathbf{K}(\hat{\mathbf{f}}) = 0$. Thus, $\mathbf{K}(\hat{\mathbf{f}}) = \mathbf{g}$ when $\hat{\mathbf{u}} = 0$.

As a representative, in what follows we prove the convergence of scheme (5.8). First of all, we give the following lemma.

Lemma 5.2. *Let the component of $\mathbf{K}(\mathbf{f})$ be defined as (1.2), and $b_{dm} > 0$ for $1 \leq d \leq D$ and $1 \leq m \leq M$. There are a family of uniformly bounded operators $R_j(\mathbf{f}, \tilde{\mathbf{f}})$ such that*

$$(5.9) \quad \nabla K_j(\mathbf{f}) = R_j(\mathbf{f}, \tilde{\mathbf{f}}) \nabla K_j(\tilde{\mathbf{f}})$$

for any $\mathbf{f}, \tilde{\mathbf{f}} \in \mathbb{R}_+^{DN}$. Furthermore, define $R(\mathbf{f}, \tilde{\mathbf{f}}) := \text{diag}(R_1(\mathbf{f}, \tilde{\mathbf{f}}), \dots, R_J(\mathbf{f}, \tilde{\mathbf{f}}))$. There exists a positive constant C_R such that

$$\|R(\mathbf{f}, \tilde{\mathbf{f}}) - I\| \leq C_R \|\mathbf{f} - \tilde{\mathbf{f}}\|.$$

Proof. The proof is referred to [Appendix A.7](#). ■

Then we have the following result.

Lemma 5.3. *Assume the conditions in [Lemma 5.2](#) hold. If $\rho_f \in (0, 1/C_R)$,*

$$(5.10) \quad \|\mathbf{K}(\mathbf{f}) - \mathbf{K}(\tilde{\mathbf{f}}) - \nabla \mathbf{K}(\tilde{\mathbf{f}})(\mathbf{f} - \tilde{\mathbf{f}})\| \leq \frac{\rho_f C_R}{1 - \rho_f C_R} \|\mathbf{K}(\mathbf{f}) - \mathbf{K}(\tilde{\mathbf{f}})\|$$

for any $\mathbf{f}, \tilde{\mathbf{f}} \in \mathcal{B}_{\tilde{\mathbf{f}}}(\rho_f)$.

Proof. See [Appendix A.8](#) for the proof. ■

In what follows we have the theorem on the convergence of scheme (5.8).

Theorem 5.4. *Assume that the conditions in [Lemma 4.5](#) and [Lemma 5.2](#) hold, and $\hat{\mathbf{u}} = 0$. Let $\rho_f \in (0, 1/C_R)$, $\rho_u > 0$, $\rho_v > 0$ and $\eta = \rho_f C_R / (1 - \rho_f C_R)$. Suppose initial point $\boldsymbol{\beta}^0$ satisfies (4.18), and step sizes τ , σ_K further satisfy*

$$(5.11) \quad \tau \sigma_K C_K^2 < (1 - \eta)s(1 - \kappa), \quad \tau < \frac{\kappa}{6L\rho_u}, \quad \sigma_K > \frac{\eta}{2(1 - \eta)}.$$

Then iterate sequence $\{\mathbf{f}^n\}$ generated by (5.8) converges to some $\hat{\mathbf{f}}'$ such that $\mathbf{K}(\hat{\mathbf{f}}') = \mathbf{g}$.

Proof. The proof is referred to [Appendix A.9](#). ■

Remark 5.5. By $\mathbf{K}(\hat{\mathbf{f}}') = \mathbf{K}(\hat{\mathbf{f}})$, $\hat{\mathbf{f}}' \in \mathcal{B}_{\hat{\mathbf{f}}}(\rho_f)$ and [Lemma 5.3](#), we get $\nabla \mathbf{K}(\hat{\mathbf{f}})(\hat{\mathbf{f}} - \hat{\mathbf{f}}') = 0$. If $\nabla \mathbf{K}(\hat{\mathbf{f}})$ is column full rank, which is available when the scan is sufficient, we obtain $\hat{\mathbf{f}}' = \hat{\mathbf{f}}$, otherwise, $\hat{\mathbf{f}}'$ is not definitely equivalent to $\hat{\mathbf{f}}$.

5.2. Numerical experiments. In this section, we describe the implementation details first, then apply the image results and evaluation metrics to show the effectiveness of the proposed algorithm framework, without loss of generality, mainly including the generated schemes in (3.7), (3.8), (3.9) and (3.10), for brevity, named EPD-Exact, EPD-Linerized, Exact-PDHGM, and Linearized-PDHGM respectively.

We adopt the simulated datasets with/without noise that generated by (1.2) to evaluate the proposed schemes for DECT. The truth image is obtained from a 2D slice of the modified 3D forbild head phantom, which is shown in the right side of [Figure 5.1](#). The water and bone basis truth images take gray values over $[0, 1]$, which are digitized by using 128×128 pixels and defined on a fixed domain $[-5, 5] \times [-5, 5]$, as shown in [Figure 5.2](#) respectively.

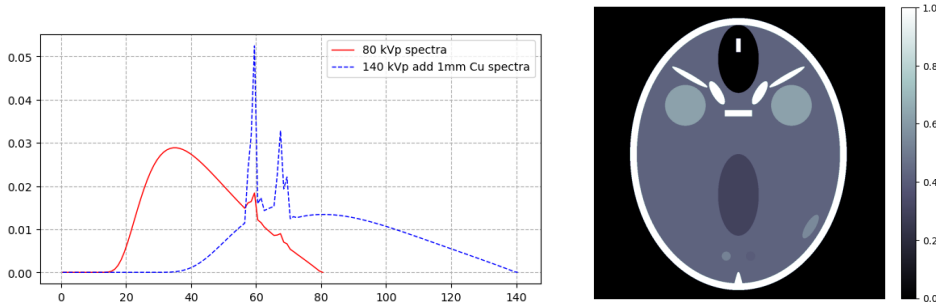


Figure 5.1: Two normalized X-ray spectra (left) and a 2D slice of the modified forbild phantom (right) used in tests.

In this paper, we assume that the used energy spectra are known, which are simulated by the software SpectrumGUI, an open source X-ray spectra simulator. We used the discrete X-ray spectra of GE Maxiray 125 X-ray tube with tube voltages 80 kVp and 140 kVp, where the 140 kVp spectra is filtered by 1 mm copper. We normalize it and use the same X-ray

spectra for different rays. The normalized spectra curve are shown in the left side of [Figure 5.1](#). The coefficients $\{b_{km}\}$ are obtained for water and bone basis materials from the database of National Institute of Standard Technology.

We perform forward/backward projections by the tool in [\[21\]](#), or calculate the projection matrix by the algorithm in [\[8\]](#). In all of the tests below, we use 2D parallel beam scanning geometry with 181 bins, which is evenly distributed on the range over $[-7.05, 7.05]$. Note that here the scanning geometry is unessential since it would only change the projection matrix. The routines were operated on ThinkStation with Xeon E5-2620 V4 2.10 GHz CPU, 64GB ROM and TITAN Xp GPU.

5.2.1. Test 1: Simulated noise-free data. For noise-free case, the measured data is simulated by $\mathbf{g} = \mathbf{K}(\mathbf{f}_{\text{truth}})$, where $\mathbf{f}_{\text{truth}}$ denotes truth image. Instead of using full-scan configuration, we consider a specific non-standard scanning configuration. The 180 views for each of low (80 kVp) and high (140 kVp) energy spectra are uniformly distributed over $[0, \pi)$ and $[\theta_0, \theta_0 + \pi)$, respectively, where constant θ_0 denotes the angular gap. Here we take it as $\pi/360$. We choose zero images as the initial point, and take $\lambda = 0$ and $\tau = \sigma_{\mathbf{K}} = 0.2$.

To validate numerical convergence, relative error, relative data fitting functional and relative TV functional are acted as convergent conditions, which are defined as

$$(5.12) \quad RE_f^{(n)} = \frac{\|\mathbf{f}^n - \mathbf{f}_{\text{truth}}\|_2}{\|\mathbf{f}_{\text{truth}}\|_2}, \quad RD_f^{(n)} = \frac{\|\mathbf{K}(\mathbf{f}^n) - \mathbf{g}\|_2^2}{\|\mathbf{g}\|_2^2}, \quad RT_f^{(n)} = \frac{|\|\nabla \mathbf{f}^n\|_1 - \|\nabla \mathbf{f}_{\text{truth}}\|_1|}{\|\nabla \mathbf{f}_{\text{truth}}\|_1},$$

respectively. These metrics can be used to verify the numerical convergence as iteration number $n \rightarrow \infty$ (also see [\[7\]](#)). Since $\mathbf{f}_{\text{truth}}$ is known in numerical simulation, the use of metrics $RE_f^{(n)}$ and $RT_f^{(n)}$ is reasonable.

After 10^6 iterations, the reconstructed water/bone basis images and 60/100 keV images are shown in the second to fifth columns of [Figure 5.2](#), which are quite close to the truth images by visual comparison.

The convergent conditions are computed by [\(5.12\)](#) for the iterative schemes and then plotted as functions of the iteration number in [Figure 5.3](#), which shows that the results reconstructed by the four schemes in [\(3.7\)](#), [\(3.8\)](#), [\(3.9\)](#) and [\(3.10\)](#) are too close to distinguish by vision. We amplify the profiles for the first 100 iterations shown in the first row of [Figure 5.3](#) and the last 100 iterations shown in the embedded subgraphs in the second row of [Figure 5.3](#).

We further use quantitative indexes to evaluate the reconstruction quality, such as the values of structural similarity (SSIM) [\[24\]](#), peak signal-to-noise ratio (PSNR), mean square error (MSE) and maximum pixel difference between the reconstructed image and corresponding truth (Max_Diff). Remark that we use ‘1 - SSIM’ instead of ‘SSIM’ because the latter value is very close to but less than 1. Since the quantitative indexes by different schemes are quite similar, we only show those produced by scheme [\(3.7\)](#) in [Table 5.1](#).

In addition, we plot the horizontal slices to compare the 60/100 keV images by scheme [\(3.7\)](#) with the truth counterparts, which are shown in [Figure 5.4](#). The locations of the slices are shown at the red line on upper left of each picture in [Figure 5.4](#).

5.2.2. Test 2: Simulated noise data. We create simulated noise data by adding Gaussian noise onto the noise-free data as in [\(1.1\)](#), which corresponds to the use of ℓ_2 data fitting term.

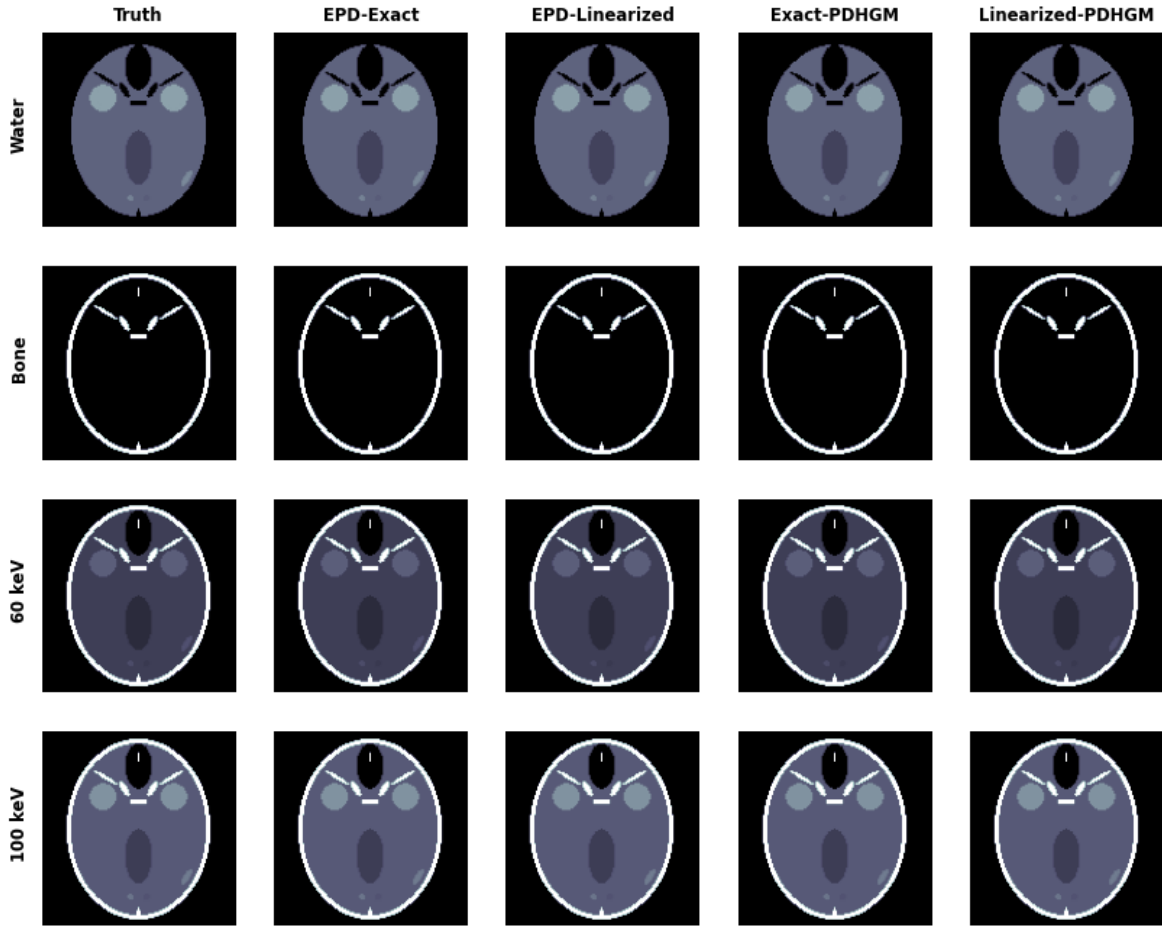


Figure 5.2: Reconstructed images after 10^6 iterations using simulated noise-free data. From left to right: truth images, reconstructed results by schemes (3.7), (3.8), (3.9) and (3.10). From top to bottom: water basis image, bone basis image, 60 keV image and 100 keV image.

The scanning configuration is the same as the simulated noise-free case in subsection 5.2.1. The signal-noise ratio (SNR) of the noise data is about 27.11 dB, and we take regularization parameter $\lambda = 10^{-6}$. We choose zero images as the initial point, and take $\tau = \sigma_K = \sigma_A = 0.2$. After 10^5 iterations, the reconstructed 60/100 keV images by schemes (3.7), (3.8), (3.9) and (3.10) are shown in Figure 5.5.

The profiles of convergent conditions for schemes (3.7), (3.8), (3.9) and (3.10) are plotted in Figure 5.6, and the last 100 iterations are shown in the embedded subgraphs of Figure 5.6. As we can see, these schemes have their own merits regarding convergence quality. The quantitative indexes of the results by scheme (3.7) are listed in Table 5.2.

Similarly, we plot the horizontal slices of the reconstructed 60/100 keV images by scheme (3.7) and the truths in Figure 5.7. We can see that the discrepancy between them is not obvious.

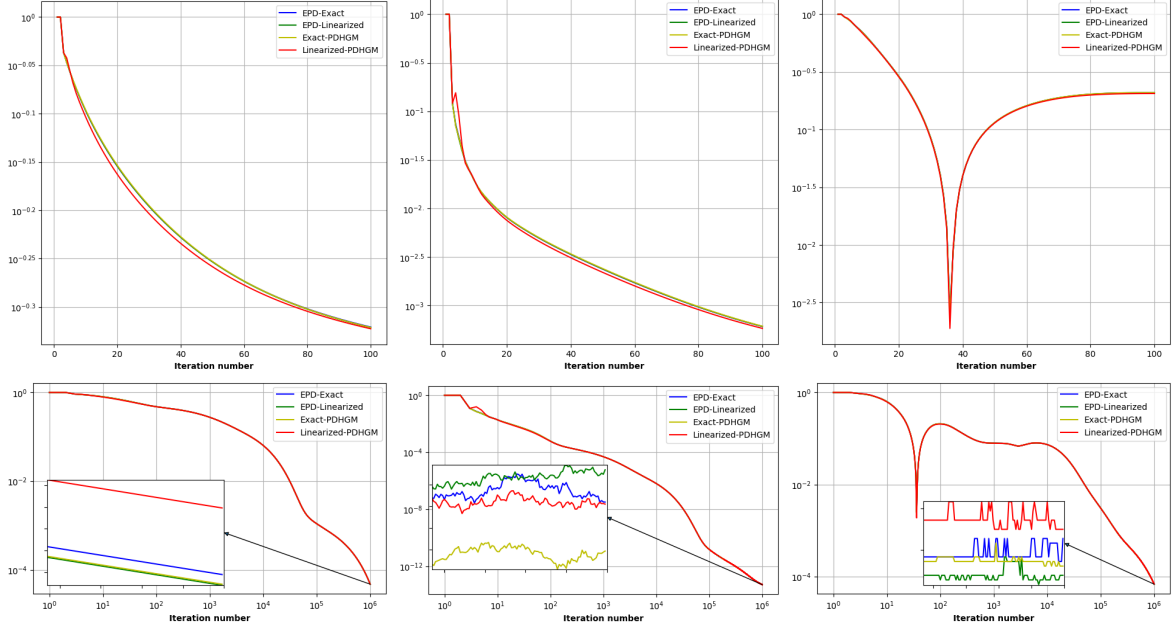


Figure 5.3: Convergent conditions $RE_f^{(n)}$ (left), $RD_f^{(n)}$ (middle) and $RT_f^{(n)}$ (right) of schemes (3.7), (3.8), (3.9) and (3.10) for simulated noise-free data, as functions of iteration number n , where the first row shows the profiles of the first 100 iterations, and the embedded subgraphs of the second row show the last 100 iterations.

Table 5.1: Quantitative indexes for the result by scheme (3.7) using simulated noise-free data.

180 views, noise-free	1-SSIM	PSNR	MSE	Max_Diff
Water basis	6.02×10^{-8}	94.60	3.47×10^{-10}	7.63×10^{-4}
Bone basis	7.51×10^{-12}	131.86	6.41×10^{-14}	5.25×10^{-6}
60 keV	4.35×10^{-9}	108.34	1.47×10^{-11}	1.57×10^{-4}
100 keV	3.04×10^{-9}	109.96	1.01×10^{-11}	1.30×10^{-4}

5.2.3. Test 3: sparse-view noise data. We test the proposed schemes with sparse-view noise data, which only contains 60 views for each low (80 kVp) and high (140 kVp) energy spectra respectively. The views of them are uniformly distributed over $[0, \pi)$ and $[\theta_0, \theta_0 + \pi)$ with $\theta_0 = \pi/120$. The noise data is generated as the way of the above test. The SNR of the data is about 27.14 dB. We take regularization parameter $\lambda = 10^{-6}$, and choose zero images as the initial point, and take $\tau = \sigma_K = \sigma_A = 0.2$. After 10^6 iterations, the reconstructed result has achieved convergence, which is shown in Figure 5.8.

The convergent conditions are shown in Figure 5.9, and the last 100 iterations are shown in the embedded subgraphs of Figure 5.9. As we can see, the convergent conditions $RE_f^{(n)}$, $RD_f^{(n)}$ and $RT_f^{(n)}$ have already converged. The performances of these schemes have only a

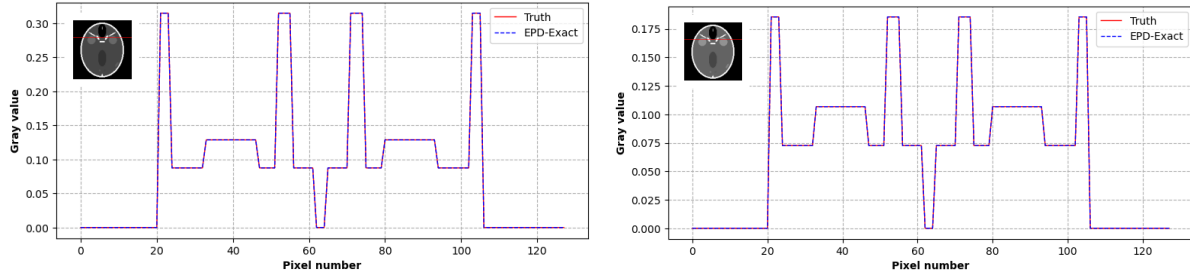


Figure 5.4: Horizontal slices of the reconstructed 60/100 keV images by scheme (3.7) and the truths for simulated noise-free data.

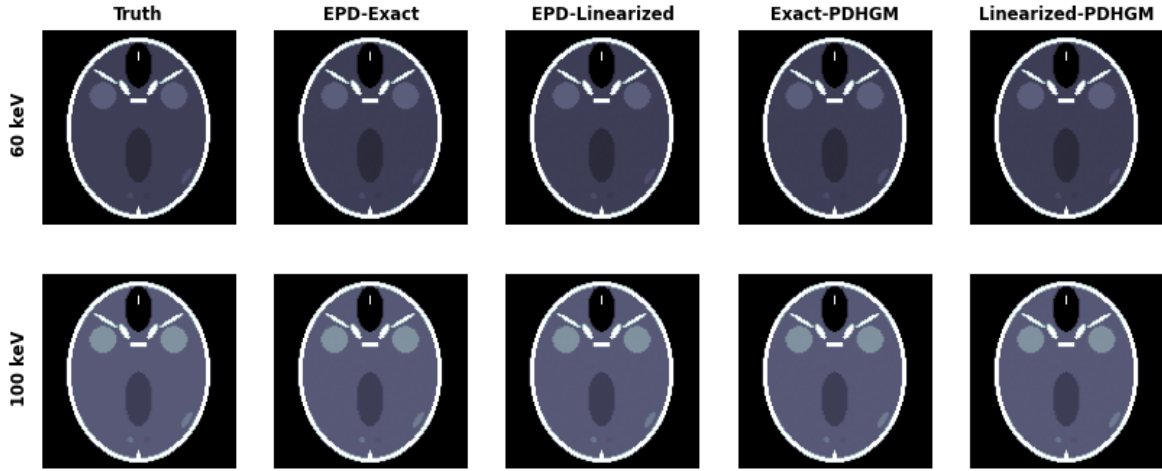


Figure 5.5: Reconstructed images after 10^5 iterations using simulated noise data (about 27.11 dB). From left to right: truth images, reconstructed results by schemes (3.7), (3.8), (3.9) and (3.10). From top to bottom: 60 keV image and 100 keV image.

little bit difference.

The quantitative indexes used to evaluate the image quality for scheme (3.7) are shown in Table 5.3, which illustrates good performance of the proposed scheme for sparse-view noise data. Furthermore, we plot the horizontal slices for the 60/100 keV images of scheme (3.7) and the truth images, which are shown in Figure 5.10. We can see that the difference between them is tiny.

6. Conclusion. In this work, we proposed an extended primal-dual algorithm framework in Algorithm 3.1 for solving a class of general nonconvex problems in (1.8) with the operator \mathbf{K} being nonlinear convex with respect to \mathbf{f} , which is motivated by the image reconstruction for several practical nonlinear imaging problems with such kind of forward operator. Note that model (1.8) also involves a kind of nonconvex sparse optimization model. Using the proposed framework, we put forward six different iterative schemes, where including the two

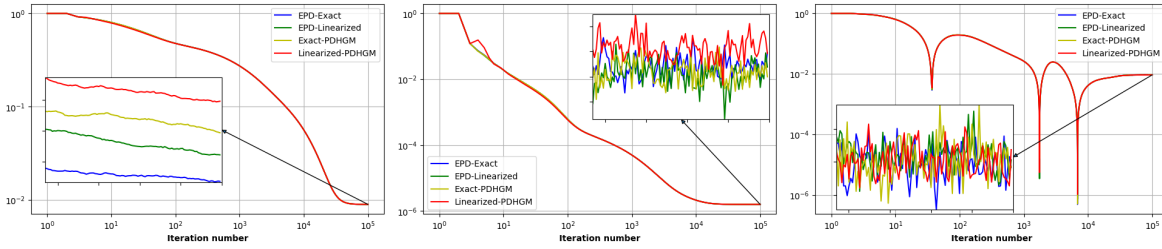


Figure 5.6: Convergent conditions $RE_f^{(n)}$ (left), $RD_f^{(n)}$ (middle) and $RT_f^{(n)}$ (right) of schemes (3.7), (3.8), (3.9) and (3.10) for simulated noise data (about 27.11 dB), as functions of iteration number n , where the embedded subgraphs of the second row show the last 100 iterations.

Table 5.2: Quantitative indexes for the results by scheme (3.7) using simulated noise data (180 views, 27.11 dB).

180 views, 27.11 dB	1-SSIM	PSNR	MSE	Max_Diff
60 keV	1.82×10^{-5}	69.51	1.12×10^{-7}	3.22×10^{-3}
100 keV	1.78×10^{-5}	70.01	9.96×10^{-8}	4.36×10^{-3}

that have been studied in the previous literatures [20, 9]. More importantly, we presented their complete mathematical explanation. We also established the relationship to existing algorithms, including primal-dual algorithm for convex problem, Exact/Linearized nonlinear PDHGM, nonconvex primal-dual algorithm, and nonconvex ADMM. With proper assumptions in subsection 4.1, we proved the convergence of these schemes when the optimal dual variable regarding the nonlinear operator is non-vanishing, where the strong convexity assumption of G is no longer required.

To demonstrate the effectiveness of the proposed algorithm framework, we applied the generated iterative schemes to solve the image reconstruction problem in (5.2) for DECT. In particular, using special properties of the concrete problem, we proved the convergence of these customized schemes when the optimal dual variable regarding the nonlinear operator is vanishing. Moreover, the numerical experiments also showed that the proposed framework has good performance on the image reconstruction problem in DECT for various data with non-standard scanning configuration.

Appendix A. Theoretical proofs.

A.1. Proof of Lemma 4.5.

Proof. By (4.4), we know $M(\mathbf{f})$ is symmetric. For any $\bar{\boldsymbol{\beta}} = [\bar{\mathbf{f}}^\top, \bar{\mathbf{u}}^\top, \bar{\mathbf{v}}^\top]^\top \in \mathcal{X} \times \mathcal{Y}_K \times \mathcal{Y}_A$,

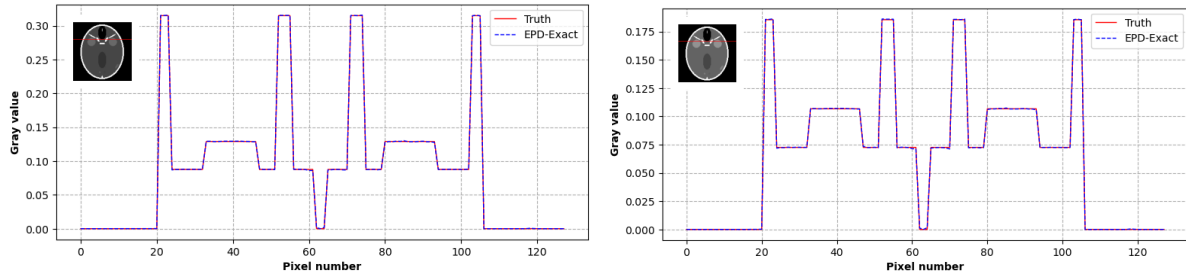


Figure 5.7: Horizontal slices of the reconstructed 60/100 keV results by scheme (3.7) and the truths for simulated noise data.

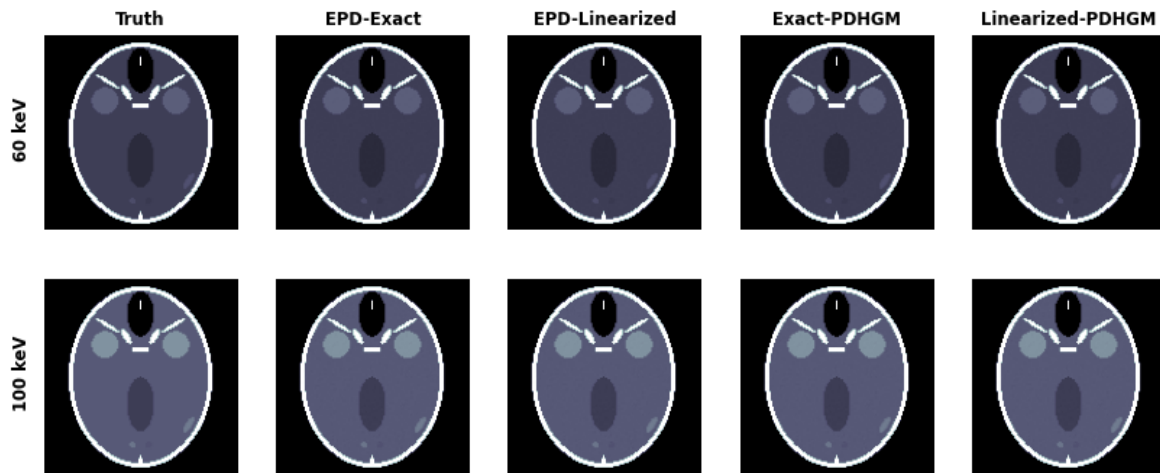


Figure 5.8: Reconstructed images after 10^6 iterations using simulated sparse-view noise data (about 27.14 dB). From left to right: truth images, reconstructed results by schemes (3.7), (3.8), (3.9) and (3.10). From top to bottom: 60 keV image and 100 keV image.

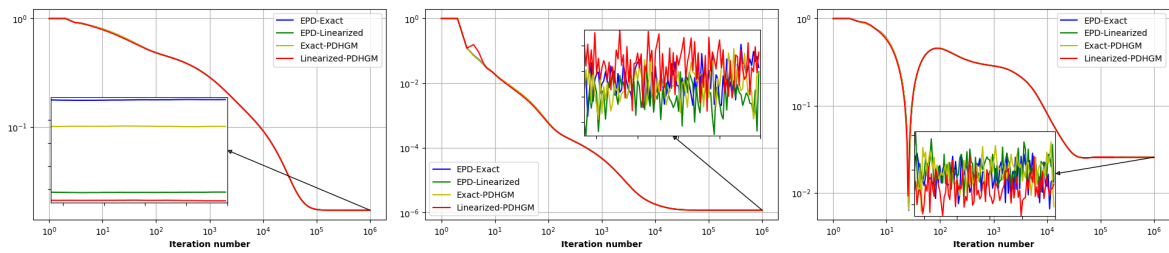


Figure 5.9: Convergent conditions $RE_f^{(n)}$ (left), $RD_f^{(n)}$ (middle) and $RT_f^{(n)}$ (right) of schemes (3.7), (3.8), (3.9) and (3.10) for simulated sparse-view noise data (about 27.14 dB), as functions of iteration number n , where the subgraphs of the second row show the last 100 iterations.

Table 5.3: Quantitative indexes for the result by scheme (3.7) using simulated sparse-view noise data (60 views, 27.14 dB).

60 views, 27.14 dB	1-SSIM	PSNR	MSE	Max_Diff
60 keV	7.75×10^{-5}	63.35	4.62×10^{-7}	6.00×10^{-3}
100 keV	7.37×10^{-5}	64.04	3.94×10^{-7}	1.03×10^{-2}

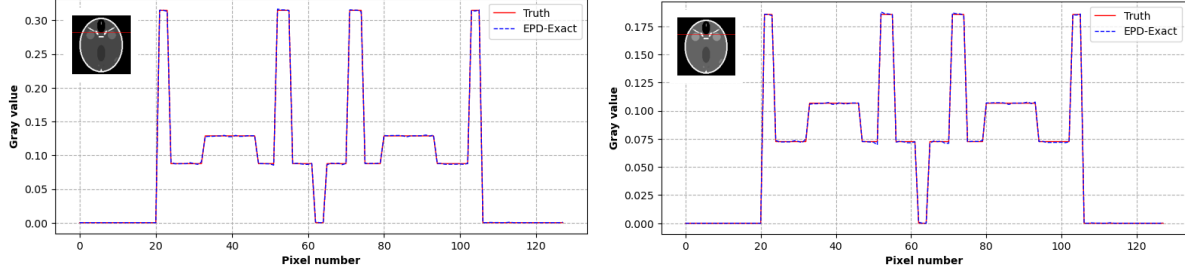


Figure 5.10: Horizontal slices of the reconstructed 60/100 keV results by scheme (3.7) and the truths for simulated sparse-view noise data.

we have

$$\begin{aligned} \bar{\beta}^\top (M(f) - B_1(f)) \bar{\beta} &= \left\| \sqrt{\frac{s(1-\kappa)}{\tau}} \bar{f} - \sqrt{\frac{\tau}{s(1-\kappa)}} [\nabla \mathbf{K}(f)]^\top \bar{\mathbf{u}} \right\|^2 \\ &\quad + \left\| \sqrt{\frac{(1-s)(1-\kappa)}{\tau}} \bar{f} - \sqrt{\frac{\tau}{(1-s)(1-\kappa)}} A^\top \bar{\mathbf{v}} \right\|^2 \geq 0. \end{aligned}$$

Moreover, by Cauchy–Schwarz inequality, we obtain

$$\bar{\beta}^\top B_1(f) \bar{\beta} \geq \frac{\delta}{\tau} \|\bar{f}\|^2 + \frac{\|\bar{\mathbf{u}}\|^2}{\sigma_K} \left(1 - \frac{\tau \sigma_K}{s(1-\kappa)} \|\nabla \mathbf{K}(f)\|^2\right) + \frac{\|\bar{\mathbf{v}}\|^2}{\sigma_A} \left(1 - \frac{\tau \sigma_A}{(1-s)(1-\kappa)} \|A\|^2\right).$$

Using (4.11), we have that the right side of the above inequality is nonnegative. Similarly, the following inequality is nonnegative

$$\bar{\beta}^\top (M(f) - B_2(f)) \bar{\beta} = \left\| \sqrt{\frac{\sigma_K}{1-\kappa}} \nabla \mathbf{K}(f) \bar{f} - \sqrt{\frac{1-\kappa}{\sigma_K}} \bar{\mathbf{u}} \right\|^2 + \left\| \sqrt{\frac{\sigma_A}{1-\kappa}} A \bar{f} - \sqrt{\frac{1-\kappa}{\sigma_A}} \bar{\mathbf{v}} \right\|^2.$$

Using Cauchy–Schwarz inequality, we obtain

$$\bar{\beta}^\top B_2(f) \bar{\beta} \geq \frac{\|\bar{f}\|^2}{\tau} \left(1 - \frac{\tau \sigma_K}{1-\kappa} \|\nabla \mathbf{K}(f)\|^2 - \frac{\tau \sigma_A}{1-\kappa} \|A\|^2\right) + \frac{\kappa}{\sigma_K} \|\bar{\mathbf{u}}\|^2 + \frac{\kappa}{\sigma_A} \|\bar{\mathbf{v}}\|^2 \geq 0.$$

Hence, we conclude the proof. ■

A.2. Proof of Lemma 4.6 .

Proof. By the definition of M_{n+1}^1 , the second term on the left side of (4.12) can be rewritten as

$$(A.1) \quad \frac{1}{2} \|\boldsymbol{\beta}^{n+1} - \widehat{\boldsymbol{\beta}}\|_{M_{n+2}^1 - M_{n+1}^1}^2 = \langle [\nabla \mathbf{K}(\mathbf{f}_\theta^n) - \nabla \mathbf{K}(\mathbf{f}_\theta^{n+1})](\mathbf{f}^{n+1} - \widehat{\mathbf{f}}), \mathbf{u}^{n+1} - \widehat{\mathbf{u}} \rangle.$$

Using the convexity of G , E^* and Assumption 1, for the first term on the left side of (4.12), we have

$$(A.2) \quad \langle \widetilde{H}_{n+1}^1(\boldsymbol{\beta}^{n+1}), \boldsymbol{\beta}^{n+1} - \widehat{\boldsymbol{\beta}} \rangle \geq \gamma_{F^*} \|\mathbf{u}^{n+1} - \widehat{\mathbf{u}}\|^2 + \langle [\nabla \mathbf{K}(\mathbf{f}_\theta^n)]^\top \mathbf{u}^{n+1} - [\nabla \mathbf{K}(\widehat{\mathbf{f}})]^\top \widehat{\mathbf{u}}, \mathbf{f}^{n+1} - \widehat{\mathbf{f}} \rangle \\ + \langle \nabla \mathbf{K}(\mathbf{f}_\theta^n)(\mathbf{f}^{n+1} - \mathbf{f}^n) - \mathbf{K}(\mathbf{f}_\theta^{n+1}) + \mathbf{K}(\widehat{\mathbf{f}}), \mathbf{u}^{n+1} - \widehat{\mathbf{u}} \rangle.$$

Then, combining (A.2) with (A.1) leads to

$$\langle \widetilde{H}_{n+1}^1(\boldsymbol{\beta}^{n+1}), \boldsymbol{\beta}^{n+1} - \widehat{\boldsymbol{\beta}} \rangle - \frac{1}{2} \|\boldsymbol{\beta}^{n+1} - \widehat{\boldsymbol{\beta}}\|_{M_{n+2}^1 - M_{n+1}^1}^2 \\ \geq \gamma_{F^*} \|\mathbf{u}^{n+1} - \widehat{\mathbf{u}}\|^2 + \langle [\nabla \mathbf{K}(\mathbf{f}_\theta^n) - \nabla \mathbf{K}(\widehat{\mathbf{f}})](\mathbf{f}^{n+1} - \widehat{\mathbf{f}}), \widehat{\mathbf{u}} \rangle \\ + \langle \mathbf{K}(\widehat{\mathbf{f}}) - \mathbf{K}(\mathbf{f}_\theta^{n+1}) - \nabla \mathbf{K}(\mathbf{f}_\theta^{n+1})(\widehat{\mathbf{f}} - \mathbf{f}_\theta^{n+1}), \mathbf{u}^{n+1} - \widehat{\mathbf{u}} \rangle \\ + \langle [\nabla \mathbf{K}(\mathbf{f}_\theta^n) - \nabla \mathbf{K}(\mathbf{f}_\theta^{n+1})](\mathbf{f}^{n+1} - \mathbf{f}^n), \mathbf{u}^{n+1} - \widehat{\mathbf{u}} \rangle.$$

Next, we estimate the above terms one by one. Using Assumption 3 and taking $\mathbf{x} = \mathbf{f}_\theta^n$, $\mathbf{f} = \mathbf{f}^{n+1}$ and $\mathbf{u} = \mathbf{u}^{n+1}$, by Cauchy–Schwarz inequality, we have the following inequality

$$\langle [\nabla \mathbf{K}(\mathbf{f}_\theta^n) - \nabla \mathbf{K}(\widehat{\mathbf{f}})](\mathbf{f}^{n+1} - \widehat{\mathbf{f}}), \widehat{\mathbf{u}} \rangle + \langle \mathbf{K}(\widehat{\mathbf{f}}) - \mathbf{K}(\mathbf{f}_\theta^{n+1}) - \nabla \mathbf{K}(\mathbf{f}_\theta^{n+1})(\widehat{\mathbf{f}} - \mathbf{f}_\theta^{n+1}), \mathbf{u}^{n+1} - \widehat{\mathbf{u}} \rangle \\ \geq -\gamma_1 \|\mathbf{u}^{n+1} - \widehat{\mathbf{u}}\|^2 - 2\lambda_1 \|\mathbf{f}^{n+1} - \mathbf{f}^n\|^2 - 2\lambda_1 \|\mathbf{f}^{n-1} - \mathbf{f}^n\|^2.$$

By mean value theorem, Assumption 2 and Cauchy–Schwarz inequality, we have

$$\langle [\mathbf{K}(\widehat{\mathbf{f}}) - \mathbf{K}(\mathbf{f}_\theta^{n+1}) - \nabla \mathbf{K}(\mathbf{f}_\theta^{n+1})(\widehat{\mathbf{f}} - \mathbf{f}_\theta^{n+1})] - [\mathbf{K}(\widehat{\mathbf{f}}) - \mathbf{K}(\mathbf{f}^{n+1}) - \nabla \mathbf{K}(\mathbf{f}^{n+1})(\widehat{\mathbf{f}} - \mathbf{f}^{n+1})], \mathbf{u}^{n+1} - \widehat{\mathbf{u}} \rangle \\ \geq -\tilde{C} \|\mathbf{f}^{n+1} - \mathbf{f}^n\|^2 - \tilde{C} \|\mathbf{u}^{n+1} - \widehat{\mathbf{u}}\|^2.$$

Using Assumption 2, triangle inequality and Cauchy–Schwarz inequality, we obtain

$$\langle [\nabla \mathbf{K}(\mathbf{f}_\theta^n) - \nabla \mathbf{K}(\mathbf{f}_\theta^{n+1})](\mathbf{f}^{n+1} - \mathbf{f}^n), \mathbf{u}^{n+1} - \widehat{\mathbf{u}} \rangle \geq -\frac{5L\rho\mathbf{u}}{2} \|\mathbf{f}^{n+1} - \mathbf{f}^n\|^2 - \frac{L\rho\mathbf{u}}{2} \|\mathbf{f}^{n-1} - \mathbf{f}^n\|^2.$$

Considering the last term on the left side of (4.12), and using Lemma 4.5, we obtain

$$\frac{1}{2} \|\boldsymbol{\beta}^{n+1} - \boldsymbol{\beta}^n\|_{M_{n+1}^1}^2 \geq \frac{\kappa}{2\tau} \|\mathbf{f}^{n+1} - \mathbf{f}^n\|^2.$$

By the above inequalities, we get (4.12) immediately.

For algorithm (3.8), similarly, we can estimate

$$\begin{aligned} & \langle \widetilde{H}_{n+1}^2(\boldsymbol{\beta}^{n+1}), \boldsymbol{\beta}^{n+1} - \widehat{\boldsymbol{\beta}} \rangle - \frac{1}{2} \|\boldsymbol{\beta}^{n+1} - \widehat{\boldsymbol{\beta}}\|_{M_{n+2}^2 - M_{n+1}^2}^2 \\ & \geq \gamma_{F^*} \|\mathbf{u}^{n+1} - \widehat{\mathbf{u}}\|^2 + \langle [\nabla \mathbf{K}(\mathbf{f}^n) - \nabla \mathbf{K}(\widehat{\mathbf{f}})](\mathbf{f}^{n+1} - \widehat{\mathbf{f}}), \widehat{\mathbf{u}} \rangle \\ & \quad + \langle \mathbf{K}(\widehat{\mathbf{f}}) - \mathbf{K}(\mathbf{f}^{n+1}) - \nabla \mathbf{K}(\mathbf{f}^{n+1})(\widehat{\mathbf{f}} - \mathbf{f}^{n+1}), \mathbf{u}^{n+1} - \widehat{\mathbf{u}} \rangle \\ & \quad + \langle [\nabla \mathbf{K}(\mathbf{f}^n) - \nabla \mathbf{K}(\mathbf{f}^{n+1})](\mathbf{f}^{n+1} - \mathbf{f}^n), \mathbf{u}^{n+1} - \widehat{\mathbf{u}} \rangle. \end{aligned}$$

Using Assumption 3, and taking $\mathbf{x} = \mathbf{f}^n$, $\mathbf{f} = \mathbf{f}^{n+1}$, $\mathbf{u} = \mathbf{u}^{n+1}$, we obtain

$$\begin{aligned} & \langle [\nabla \mathbf{K}(\mathbf{f}^n) - \nabla \mathbf{K}(\widehat{\mathbf{f}})](\mathbf{f}^{n+1} - \widehat{\mathbf{f}}), \widehat{\mathbf{u}} \rangle + \langle \mathbf{K}(\widehat{\mathbf{f}}) - \mathbf{K}(\mathbf{f}^{n+1}) - \nabla \mathbf{K}(\mathbf{f}^{n+1})(\widehat{\mathbf{f}} - \mathbf{f}^{n+1}), \mathbf{u}^{n+1} - \widehat{\mathbf{u}} \rangle \\ & \geq -\gamma_1 \|\mathbf{u}^{n+1} - \widehat{\mathbf{u}}\|^2 - \lambda_1 \|\mathbf{f}^{n+1} - \mathbf{f}^n\|^2. \end{aligned}$$

By Assumption 2, it is easy to obtain that

$$\langle [\nabla \mathbf{K}(\mathbf{f}^n) - \nabla \mathbf{K}(\mathbf{f}^{n+1})](\mathbf{f}^{n+1} - \mathbf{f}^n), \mathbf{u}^{n+1} - \widehat{\mathbf{u}} \rangle \geq -L\rho_{\mathbf{u}} \|\mathbf{f}^{n+1} - \mathbf{f}^n\|^2.$$

Moreover,

$$\frac{1}{2} \|\boldsymbol{\beta}^{n+1} - \boldsymbol{\beta}^n\|_{M_{n+1}^2}^2 \geq \frac{\kappa}{2\tau} \|\mathbf{f}^{n+1} - \mathbf{f}^n\|^2.$$

Using the above results, we have (4.13). ■

A.3. Proof of Corollary 4.7.

Proof. Considering the first step of algorithm (3.7), due to $\bar{\mathbf{f}}^0 = \mathbf{f}^0$ and $\gamma_{F^*} - \gamma_1 - \tilde{C} > 0$, by (4.12) and Theorem 4.4, we get

$$\frac{1}{2} \|\boldsymbol{\beta}^1 - \widehat{\boldsymbol{\beta}}\|_{M_2^1}^2 \leq \frac{1}{2} \|\boldsymbol{\beta}^0 - \widehat{\boldsymbol{\beta}}\|_{M_1^1}^2 - \Lambda_1(\tau) \|\mathbf{f}^1 - \mathbf{f}^0\|^2.$$

The assumption (4.14) implies that $\Lambda_1(\tau) > 2\lambda_1 + L\rho_{\mathbf{u}}/2$. Then, when $N \geq 1$, by (4.10), we have

$$\begin{aligned} & \frac{1}{2} \|\boldsymbol{\beta}^{N+1} - \widehat{\boldsymbol{\beta}}\|_{M_{N+2}^1}^2 - \frac{1}{2} \|\boldsymbol{\beta}^0 - \widehat{\boldsymbol{\beta}}\|_{M_1^1}^2 \\ & \leq - \sum_{n=0}^{N-1} \left(\Lambda_1(\tau) - \left(2\lambda_1 + \frac{L\rho_{\mathbf{u}}}{2} \right) \right) \|\mathbf{f}^{n+1} - \mathbf{f}^n\|^2 - \Lambda_1(\tau) \|\mathbf{f}^{N+1} - \mathbf{f}^N\|^2 \leq 0, \end{aligned}$$

which implies (4.15).

Next, for algorithm (3.8), by (4.13) and Theorem 4.4, we obtain

$$\frac{1}{2} \|\boldsymbol{\beta}^{n+1} - \widehat{\boldsymbol{\beta}}\|_{M_{n+2}^2}^2 \leq \frac{1}{2} \|\boldsymbol{\beta}^n - \widehat{\boldsymbol{\beta}}\|_{M_{n+1}^2}^2 - \Lambda_2(\tau) \|\mathbf{f}^{n+1} - \mathbf{f}^n\|^2.$$

Then the condition (4.16) implies that $\Lambda_2(\tau) > 0$. Hence, (4.17) is proved. ■

A.4. Proof of Lemma 4.8.

Proof. We begin the proof by estimating the distances from $\mathbf{f}^{n+1}, \mathbf{f}^n$ to $\widehat{\mathbf{f}}$. Using (4.1) yields that

$$(A.3) \quad \widehat{\mathbf{f}} = (\text{Id} + \tau \partial G)^{-1}(\widehat{\mathbf{f}} - \tau [\nabla \mathbf{K}(\widehat{\mathbf{f}})]^\top \widehat{\mathbf{u}} - \tau A^\top \widehat{\mathbf{v}}),$$

$$(A.4) \quad \widehat{\mathbf{u}} = (\text{Id} + \sigma_K \partial F^*)^{-1}(\widehat{\mathbf{u}} + \sigma_K \mathbf{K}(\widehat{\mathbf{f}})),$$

$$(A.5) \quad \widehat{\mathbf{v}} = (\text{Id} + \sigma_A \partial E^*)^{-1}(\widehat{\mathbf{v}} + \sigma_A A \widehat{\mathbf{f}}).$$

Using (3.7a) and (A.3), by Proposition 2.5, we obtain

$$(A.6) \quad \|\mathbf{f}^{n+1} - \widehat{\mathbf{f}}\| \leq \|\mathbf{f}^n - \widehat{\mathbf{f}}\| + C_f^n,$$

where $C_f^n := \tau \|[\nabla \mathbf{K}(\mathbf{f}_\theta^n)]^\top \mathbf{u}^n - [\nabla \mathbf{K}(\widehat{\mathbf{f}})]^\top \widehat{\mathbf{u}} + A^\top (\mathbf{v}^n - \widehat{\mathbf{v}})\|$. Similarly, we obtain the following results

$$\|\mathbf{u}^{n+1} - \widehat{\mathbf{u}}\| \leq \|\mathbf{u}^n - \widehat{\mathbf{u}}\| + C_u^n \quad \text{and} \quad \|\mathbf{v}^{n+1} - \widehat{\mathbf{v}}\| \leq \|\mathbf{v}^n - \widehat{\mathbf{v}}\| + C_v^n,$$

where $C_u^n := \sigma_K \|\mathbf{K}(\mathbf{f}_\theta^{n+1}) - \mathbf{K}(\widehat{\mathbf{f}})\|$ and $C_v^n := \sigma_A \|A \mathbf{f}_\theta^{n+1} - A \widehat{\mathbf{f}}\|$, respectively. Hence we prove a stronger conclusion $\{\boldsymbol{\beta}^n\}_{n \in \mathbb{N}} \subset \mathcal{O}(r_f, r_u, r_v)$ than $\{\boldsymbol{\beta}^n\}_{n \in \mathbb{N}} \subseteq \mathcal{O}(\rho_f, \rho_u, \rho_v)$ by induction.

Firstly we consider the initial step, by $\boldsymbol{\beta}^0 \in \mathcal{O}(r_f, r_u, r_v)$,

$$C_f^0 \leq \tau (\|[\nabla \mathbf{K}(\mathbf{f}^0)]^\top (\mathbf{u}^0 - \widehat{\mathbf{u}}) + [\nabla \mathbf{K}(\mathbf{f}^0) - \nabla \mathbf{K}(\widehat{\mathbf{f}})]^\top \widehat{\mathbf{u}}\| + \|A^\top (\mathbf{v}^0 - \widehat{\mathbf{v}})\|) \leq C_f,$$

where $C_f := \tau ((r_u + 2\|\widehat{\mathbf{u}}\|)C_K + \|A\|r_v)$. By the convexity of G and Proposition 2.5, we have

$$\langle (\mathbf{f}^n - \tau [\nabla \mathbf{K}(\mathbf{f}_\theta^n)]^\top \mathbf{u}^n - \tau A^\top \mathbf{v}^n) - (\widehat{\mathbf{f}} - \tau [\nabla \mathbf{K}(\widehat{\mathbf{f}})]^\top \widehat{\mathbf{u}} - \tau A^\top \widehat{\mathbf{v}}), \mathbf{f}^{n+1} - \widehat{\mathbf{f}} \rangle \geq \|\mathbf{f}^{n+1} - \widehat{\mathbf{f}}\|^2$$

for all n . By the above inequality,

$$\begin{aligned} & \|\mathbf{f}^{n+1} - \widehat{\mathbf{f}}\|^2 + \|\mathbf{f}^{n+1} - \mathbf{f}^n\|^2 - \|\mathbf{f}^n - \widehat{\mathbf{f}}\|^2 \\ &= 2(\|\mathbf{f}^{n+1} - \widehat{\mathbf{f}}\|^2 - \langle \mathbf{f}^n - \widehat{\mathbf{f}}, \mathbf{f}^{n+1} - \widehat{\mathbf{f}} \rangle) \\ &\leq 2\tau \langle -[\nabla \mathbf{K}(\mathbf{f}_\theta^n)]^\top \mathbf{u}^n + [\nabla \mathbf{K}(\widehat{\mathbf{f}})]^\top \widehat{\mathbf{u}} - A^\top \mathbf{v}^n + A^\top \widehat{\mathbf{v}}, \mathbf{f}^{n+1} - \widehat{\mathbf{f}} \rangle \\ &\leq 2C_f^n \|\mathbf{f}^{n+1} - \widehat{\mathbf{f}}\|, \end{aligned}$$

which holds for all n .

By the above estimate and (A.6), for \mathbf{f}_θ^1 , we have

$$\begin{aligned} \|\mathbf{f}_\theta^1 - \widehat{\mathbf{f}}\|^2 &= 2(\|\mathbf{f}^1 - \widehat{\mathbf{f}}\|^2 + \|\mathbf{f}^1 - \mathbf{f}^0\|^2) - \|\mathbf{f}^0 - \widehat{\mathbf{f}}\|^2 \\ &\leq 4C_f^0 \|\mathbf{f}^1 - \widehat{\mathbf{f}}\| + \|\mathbf{f}^0 - \widehat{\mathbf{f}}\|^2 \\ &\leq 4C_f^0 (\|\mathbf{f}^0 - \widehat{\mathbf{f}}\| + C_f^0) + \|\mathbf{f}^0 - \widehat{\mathbf{f}}\|^2 \\ &= (\|\mathbf{f}^0 - \widehat{\mathbf{f}}\| + 2C_f^0)^2 \\ &\leq (r_f + 2C_f)^2, \end{aligned}$$

which illustrates $\mathbf{f}_\theta^1 \in \mathcal{B}_{\widehat{\mathbf{f}}}(r_f + 2C_f)$. Therefore,

$$C_u^0 = \sigma_K \|\mathbf{K}(\mathbf{f}_\theta^1) - \mathbf{K}(\widehat{\mathbf{f}})\| \leq \sigma_K (r_f + 2C_f) C_K = C_u.$$

Similarly, $C_v^0 \leq C_v$. Thus, when $n = 1$, the induction proposition holds. Now suppose that induction assumption holds with $1 \leq n \leq N$, which is

$$(A.7) \quad \boldsymbol{\beta}^n \in \mathcal{O}(r_f, r_u, r_v), \quad C_f^{n-1} \leq C_f, \quad C_u^{n-1} \leq C_u, \quad C_v^{n-1} \leq C_v.$$

Next we proof the case for $n = N + 1$. One needs to pay attention to the order of proof here. Firstly,

$$\begin{aligned} C_f^N &= \tau \|\nabla \mathbf{K}(\mathbf{f}^N)\|^\top \mathbf{u}^N - \nabla \mathbf{K}(\widehat{\mathbf{f}})\|^\top \widehat{\mathbf{u}} + A^\top (\mathbf{v}^N - \widehat{\mathbf{v}})\| \\ &\leq \tau (\|\nabla \mathbf{K}(\mathbf{f}^N)\|^\top (\mathbf{u}^N - \widehat{\mathbf{u}}) + \|\nabla \mathbf{K}(\mathbf{f}^N) - \nabla \mathbf{K}(\widehat{\mathbf{f}})\|^\top \widehat{\mathbf{u}} + \|A^\top (\mathbf{v}^N - \widehat{\mathbf{v}})\|) \\ &\leq \tau ((r_u + 2\|\widehat{\mathbf{u}}\|)C_K + \|A\|r_v) = C_f. \end{aligned}$$

Then,

$$\|\mathbf{f}_\theta^{N+1} - \widehat{\mathbf{f}}\|^2 = 2(\|\mathbf{f}^{N+1} - \widehat{\mathbf{f}}\|^2 + \|\mathbf{f}^{N+1} - \mathbf{f}^N\|^2) - \|\mathbf{f}^N - \widehat{\mathbf{f}}\|^2 \leq (r_f + 2C_f)^2.$$

Similarly, we obtain

$$C_u^N = \sigma_K \|\mathbf{K}(\mathbf{f}_\theta^{N+1}) - \mathbf{K}(\widehat{\mathbf{f}})\| \leq \sigma_K (r_f + 2C_f) C_K = C_u,$$

and $C_v^N \leq C_v$. Together with the estimate (A.6), we have

$$\|\mathbf{f}^{N+1} - \widehat{\mathbf{f}}\| \leq \|\mathbf{f}^N - \widehat{\mathbf{f}}\| + C_f^N \leq r_f + C_f^N \leq r_f + C_f,$$

which shows that $\mathbf{f}^{N+1} \in \mathcal{B}_{\widehat{\mathbf{f}}}(r_f + C_f)$. Similarly, we have $\mathbf{u}^{N+1} \in \mathcal{B}_{\widehat{\mathbf{u}}}(r_u + C_u)$ and $\mathbf{v}^{N+1} \in \mathcal{B}_{\widehat{\mathbf{v}}}(r_v + C_v)$. These give $\boldsymbol{\beta}^{N+1} \in \mathcal{O}(\rho_f, \rho_u, \rho_v)$. Then by Corollary 4.7, we obtain $\|\boldsymbol{\beta}^{N+1} - \widehat{\boldsymbol{\beta}}\|_{M_{N+2}^1} \leq \|\boldsymbol{\beta}^0 - \widehat{\boldsymbol{\beta}}\|_{M_1^1}$. Using Lemma 4.5, we have

$$\begin{aligned} \|\boldsymbol{\beta}^{N+1} - \widehat{\boldsymbol{\beta}}\|_{M_{N+2}^1}^2 &\geq \max \left\{ \|\boldsymbol{\beta}^{N+1} - \widehat{\boldsymbol{\beta}}\|_{B_1(\mathbf{f}_\theta^{N+1})}^2, \|\boldsymbol{\beta}^{N+1} - \widehat{\boldsymbol{\beta}}\|_{B_2(\mathbf{f}_\theta^{N+1})}^2 \right\} \\ &\geq \max \left\{ \frac{\kappa}{\tau} \|\mathbf{f}^{N+1} - \widehat{\mathbf{f}}\|^2, \frac{\kappa}{\sigma_K} \|\mathbf{u}^{N+1} - \widehat{\mathbf{u}}\|^2, \frac{\kappa}{\sigma_A} \|\mathbf{v}^{N+1} - \widehat{\mathbf{v}}\|^2 \right\}. \end{aligned}$$

Thus, together with (4.18), we obtain

$$\|\mathbf{f}^{N+1} - \widehat{\mathbf{f}}\| \leq \frac{\|\boldsymbol{\beta}^{N+1} - \widehat{\boldsymbol{\beta}}\|_{M_{N+2}^1}}{\sqrt{\kappa/\tau}} \leq \frac{\|\boldsymbol{\beta}^0 - \widehat{\boldsymbol{\beta}}\|_{M_1^1}}{\sqrt{\kappa/\tau}} \leq r_f.$$

Similarly, we have

$$\|\mathbf{u}^{N+1} - \widehat{\mathbf{u}}\| \leq \frac{\|\boldsymbol{\beta}^{N+1} - \widehat{\boldsymbol{\beta}}\|_{M_{N+2}^1}}{\sqrt{\kappa/\sigma_K}} \leq \frac{\|\boldsymbol{\beta}^0 - \widehat{\boldsymbol{\beta}}\|_{M_1^1}}{\sqrt{\kappa/\sigma_K}} \leq r_u,$$

and $\|\mathbf{v}^{N+1} - \widehat{\mathbf{v}}\| \leq r_v$. Therefore $\boldsymbol{\beta}^{N+1} \in \mathcal{O}(r_f, r_u, r_v)$, and the assumption of induction holds. Hence we complete the proof. \blacksquare

A.5. Proof of Theorem 4.9.

Proof. By Lemma 4.8, iterate points $\boldsymbol{\beta}^n, \boldsymbol{\beta}^{n+1} \in \mathcal{O}(\rho_f, \rho_u, \rho_v)$ and $\mathbf{f}_\theta^{n+1} \in \mathcal{B}_{\tilde{f}}(\rho_f)$. Using Lemma 4.6, we obtain (4.12). By Theorem 4.4, for all $n \geq 1$,

$$\begin{aligned} \frac{1}{2} \|\boldsymbol{\beta}^n - \widehat{\boldsymbol{\beta}}\|_{M_{n+1}^1}^2 - \frac{1}{2} \|\boldsymbol{\beta}^{n+1} - \widehat{\boldsymbol{\beta}}\|_{M_{n+2}^1}^2 &\geq (\gamma_{F^*} - \gamma_1 - \tilde{C}) \|\mathbf{u}^{n+1} - \widehat{\mathbf{u}}\|^2 \\ &\quad + \Lambda_1(\tau) \|\mathbf{f}^{n+1} - \mathbf{f}^n\|^2 - (2\lambda_1 + \frac{L\rho_u}{2}) \|\mathbf{f}^{n-1} - \mathbf{f}^n\|^2. \end{aligned}$$

Specially for the case of $n = 0$, since $\bar{\mathbf{f}}^0 = \mathbf{f}^0$, we have

$$\frac{1}{2} \|\boldsymbol{\beta}^0 - \widehat{\boldsymbol{\beta}}\|_{M_1^1}^2 - \frac{1}{2} \|\boldsymbol{\beta}^1 - \widehat{\boldsymbol{\beta}}\|_{M_2^1}^2 \geq (\gamma_{F^*} - \gamma_1) \|\mathbf{u}^1 - \widehat{\mathbf{u}}\|^2 + \Lambda_1(\tau) \|\mathbf{f}^1 - \mathbf{f}^0\|^2.$$

Summarizing the above estimate inequalities over $n = 0, \dots, N$, we obtain

$$\begin{aligned} &\frac{1}{2} \|\boldsymbol{\beta}^0 - \widehat{\boldsymbol{\beta}}\|_{M_1^1}^2 - \frac{1}{2} \|\boldsymbol{\beta}^{N+1} - \widehat{\boldsymbol{\beta}}\|_{M_{N+2}^1}^2 \\ &\geq (\gamma_{F^*} - \gamma_1 - \tilde{C}) \sum_{n=0}^N \|\mathbf{u}^{n+1} - \widehat{\mathbf{u}}\|^2 + \Lambda_1(\tau) \|\mathbf{f}^1 - \mathbf{f}^0\|^2 \\ &\quad + \sum_{n=1}^N \left[\Lambda_1(\tau) \|\mathbf{f}^{n+1} - \mathbf{f}^n\|^2 - (2\lambda_1 + \frac{L\rho_u}{2}) \|\mathbf{f}^n - \mathbf{f}^{n-1}\|^2 \right] \\ &= (\gamma_{F^*} - \gamma_1 - \tilde{C}) \sum_{n=0}^N \|\mathbf{u}^{n+1} - \widehat{\mathbf{u}}\|^2 + \Lambda_1(\tau) \|\mathbf{f}^{N+1} - \mathbf{f}^N\|^2 \\ &\quad + \left(\Lambda_1(\tau) - (2\lambda_1 + \frac{L\rho_u}{2}) \right) \sum_{n=0}^{N-1} \|\mathbf{f}^{n+1} - \mathbf{f}^n\|^2. \end{aligned}$$

Recall that $\boldsymbol{\beta}^{N+1} \in \mathcal{O}(r_f, r_u, r_v)$ for all $N \in \mathbb{N}$ in Lemma 4.8 and (4.18), we obtain that the left side of above inequality is bounded. Thus

$$\left(\Lambda_1(\tau) - (2\lambda_1 + \frac{L\rho_u}{2}) \right) \sum_{n=0}^{N-1} \|\mathbf{f}^{n+1} - \mathbf{f}^n\|^2 < \infty.$$

The condition (4.14) implies that $\Lambda_1(\tau) > (2\lambda_1 + \frac{L\rho_u}{2})$, consequently,

$$\sum_{n=0}^{N-1} \|\mathbf{f}^{n+1} - \mathbf{f}^n\|^2 < \infty,$$

which illustrates that $\{\mathbf{f}^n\}_{n \in \mathbb{N}}$ is a Cauchy sequence. Since \mathcal{X} is a finite dimensional Euclidean space, it follows that $\{\mathbf{f}^n\}_{n \in \mathbb{N}}$ converges to some $\tilde{\mathbf{f}}' \in \mathcal{B}_{\tilde{f}}(r_f)$. Similarly, $\{\mathbf{v}^n\}_{n \in \mathbb{N}}$ converges to $\tilde{\mathbf{v}}' \in \mathcal{B}_{\tilde{v}}(r_v)$. Moreover, by strongly monotone factor $\gamma_{F^*} > \gamma_1 + \tilde{C}$, we obtain $\{\mathbf{u}^n\}_{n \in \mathbb{N}}$ converges

to $\widehat{\mathbf{u}}$. Recall the iteration formula of (3.7), let $N \rightarrow \infty$, we obtain

$$0 \in \begin{bmatrix} \partial G(\widehat{\mathbf{f}}') + [\nabla \mathbf{K}(\widehat{\mathbf{f}}')]^\top \widehat{\mathbf{u}} + A^\top \widehat{\mathbf{v}}' \\ \partial F^*(\widehat{\mathbf{u}}) - \mathbf{K}(\widehat{\mathbf{f}}') \\ \partial E^*(\widehat{\mathbf{v}}') - A(\widehat{\mathbf{f}}') \end{bmatrix},$$

which is the desired result. ■

A.6. Proof of Theorem 5.1.

Proof. Obviously, K_j is Fréchet differentiable. Let $\mathbf{b}_d = [b_{d1}, \dots, b_{dM}]^\top \in \mathbb{R}^M$ for $d = 1, \dots, D$. We further define

$$z_{jm}(\mathbf{f}) := -\sum_{d=1}^D b_{dm} \mathbf{a}_j^\top \mathbf{f}_d, \quad \mathbf{z}_j(\mathbf{f}) := [z_{j1}(\mathbf{f}), \dots, z_{jM}(\mathbf{f})]^\top$$

and sometimes use z_{jm} and \mathbf{z}_j without \mathbf{f} for simplicity.

Let

$$\exp(\mathbf{z}_j) := [\exp(z_{j1}), \dots, \exp(z_{jM})]^\top.$$

Then we can reformulate (1.2) as $K_j(\mathbf{f}) = \ln \sum_{m=1}^M s_{jm} \exp(z_{jm})$. Direct calculation yields

$$(A.8) \quad \frac{\partial K_j(\mathbf{f})}{\partial \mathbf{z}_j} = \frac{\mathbf{s}_j \odot \exp(\mathbf{z}_j)}{\mathbf{s}_j^\top \exp(\mathbf{z}_j)} =: \bar{\omega}_j(\mathbf{f}),$$

where \odot denotes the element-wise product between two same-dimensional vectors. By the chain rule,

$$(A.9) \quad \nabla_{\mathbf{f}_d} K_j(\mathbf{f}) = \sum_{m=1}^M \frac{\partial K_j(\mathbf{f})}{\partial z_{jm}} \frac{\partial z_{jm}}{\partial \mathbf{f}_d} = -(\bar{\omega}_j(\mathbf{f}))^\top \mathbf{b}_d \mathbf{a}_j.$$

To compute the Hessian matrix of $K_j(\mathbf{f})$, we further let

$$(A.10) \quad \zeta_{jm} := s_{jm} \exp(z_{jm}),$$

and derive

$$\nabla_{\mathbf{f}_d \mathbf{f}_e}^2 K_j(\mathbf{f}) = \frac{\mathbf{a}_j \mathbf{a}_j^\top}{(\mathbf{s}_j^\top \exp(\mathbf{z}_j))^2} \sum_{m < n}^M \zeta_{jm} \zeta_{jn} (b_{dm} - b_{dn})(b_{em} - b_{en}) =: \alpha_{de}(\mathbf{f}) \mathbf{a}_j \mathbf{a}_j^\top.$$

For any $\mathbf{u} = [\mathbf{u}_1^\top, \dots, \mathbf{u}_D^\top]^\top$ with $\mathbf{u}_d \in \mathbb{R}^N$ for $d = 1, \dots, D$,

$$\mathbf{u}^\top \nabla^2 K_j(\mathbf{f}) \mathbf{u} = \frac{1}{(\mathbf{s}_j^\top \exp(\mathbf{z}_j))^2} \sum_{m < n}^M \sum_{d,e}^D \zeta_{jm} \zeta_{jn} \left[\mathbf{a}_j^\top \mathbf{u}_d (b_{dm} - b_{dn}) + \mathbf{a}_j^\top \mathbf{u}_e (b_{em} - b_{en}) \right]^2 \geq 0,$$

which illustrates that $\nabla^2 K_j(\mathbf{f})$ is positive semidefinite. Hence, $K_j(\mathbf{f})$ is convex. Subsequently, for any $\mathbf{f} \in \mathbb{R}^{DN}$, the maximum eigenvalue of $\nabla K_j(\mathbf{f})$ satisfies

$$\mu_{\max} \leq \|\mathbf{a}_j\|^2 \sum_{d=1}^D \alpha_{dd}(\mathbf{f}) < \infty,$$

which shows that ∇K_j is global Lipschitz continuous. ■

A.7. Proof of Lemma 5.2.

Proof. By (A.9), we know

$$\nabla K_j(\mathbf{f}) = \begin{bmatrix} -(\bar{\omega}_j(\mathbf{f})^\top \mathbf{b}_1) \mathbf{a}_j \\ \vdots \\ -(\bar{\omega}_j(\mathbf{f})^\top \mathbf{b}_D) \mathbf{a}_j \end{bmatrix}.$$

Hence, there is a solution to (5.9) as

$$R_j(\mathbf{f}, \tilde{\mathbf{f}}) = \text{diag}\left(\frac{\bar{\omega}_j(\mathbf{f})^\top \mathbf{b}_1}{\bar{\omega}_j(\tilde{\mathbf{f}})^\top \mathbf{b}_1} \text{Id}, \dots, \frac{\bar{\omega}_j(\mathbf{f})^\top \mathbf{b}_d}{\bar{\omega}_j(\tilde{\mathbf{f}})^\top \mathbf{b}_d} \text{Id}\right).$$

Due to the soft-max structure of $\bar{\omega}_j(\mathbf{f})$ in (A.8) and positivity of \mathbf{b}_d ,

$$\frac{\min_m b_{dm}}{\max_m b_{dm}} \leq \frac{\bar{\omega}_j(\mathbf{f})^\top \mathbf{b}_d}{\bar{\omega}_j(\tilde{\mathbf{f}})^\top \mathbf{b}_d} \leq \frac{\max_m b_{dm}}{\min_m b_{dm}}$$

for any $\mathbf{f}, \tilde{\mathbf{f}} \in \mathbb{R}_+^{DN}$, which implies that the eigenvalues of $R_j(\mathbf{f}, \tilde{\mathbf{f}})$ have uniform bound. By mean value theorem and Cauchy–Schwarz inequality, we have

$$\|R_j(\mathbf{f}, \tilde{\mathbf{f}}) - \text{Id}\|_2 \leq \max_d \frac{\|\mathbf{b}_d\|}{\min_m b_{dm}} \|\nabla \bar{\omega}_j(\xi \mathbf{f} + (1 - \xi) \tilde{\mathbf{f}})\| \|\mathbf{f} - \tilde{\mathbf{f}}\|.$$

Furthermore, by the definitions in (A.8) and (A.10), for any $\mathbf{f} \in \mathbb{R}_+^{DN}$, we have

$$\begin{aligned} \|\nabla \bar{\omega}_j(\mathbf{f})\| &\leq \sum_{d=1}^D \sum_{m=1}^M \sum_{n=1}^M \frac{\zeta_{jm} \zeta_{jn} |b_{dn} - b_{dm}| \|\mathbf{a}_j\|}{\left(\mathbf{s}_j^\top \exp(\mathbf{z}_j)\right)^2} \\ &\leq \sum_{d=1}^D \max_{m,n} |b_{dm} - b_{dn}| \|\mathbf{a}_j\|. \end{aligned}$$

By the definition of $R(\mathbf{f}, \tilde{\mathbf{f}})$, and using the above estimates, we have

$$\begin{aligned} \|R(\mathbf{f}, \tilde{\mathbf{f}}) - I\|_2 &= \max_j \|R_j(\mathbf{f}) - I\|_2 \\ &\leq \sum_{d=1}^D \max_{m,n} |b_{dm} - b_{dn}| \max_d \frac{\|\mathbf{b}_d\|}{\min_m b_{dm}} \max_j \|\mathbf{a}_j\| \|\mathbf{f} - \tilde{\mathbf{f}}\|, \end{aligned}$$

which concludes the proof. ■

A.8. Proof of Lemma 5.3.

Proof. By Lemma 5.2, we have

$$\begin{aligned}
\|\mathbf{K}(\mathbf{f}) - \mathbf{K}(\tilde{\mathbf{f}}) - \nabla\mathbf{K}(\tilde{\mathbf{f}})(\mathbf{f} - \tilde{\mathbf{f}})\| &= \left\| \int_0^1 (\nabla\mathbf{K}(\mathbf{f}_t) - \nabla\mathbf{K}(\tilde{\mathbf{f}}))(\mathbf{f} - \tilde{\mathbf{f}}) dt \right\| \\
&\leq \int_0^1 \|(R(\mathbf{f}_t, \tilde{\mathbf{f}}) - I)\nabla\mathbf{K}(\tilde{\mathbf{f}})(\mathbf{f} - \tilde{\mathbf{f}})\| dt \\
&\leq \left(\int_0^1 C_R \|\mathbf{f}_t - \tilde{\mathbf{f}}\| dt \right) \|\nabla\mathbf{K}(\tilde{\mathbf{f}})(\mathbf{f} - \tilde{\mathbf{f}})\| \\
&= \frac{1}{2} C_R \|\mathbf{f} - \tilde{\mathbf{f}}\| \|\nabla\mathbf{K}(\tilde{\mathbf{f}})(\mathbf{f} - \tilde{\mathbf{f}})\|,
\end{aligned}$$

where $\mathbf{f}_t := t\mathbf{f} + (1-t)\tilde{\mathbf{f}}$. Using $\mathbf{f}, \tilde{\mathbf{f}} \in \mathcal{B}_{\tilde{\mathbf{f}}}(\rho)$ yields that

$$\|\mathbf{K}(\mathbf{f}) - \mathbf{K}(\tilde{\mathbf{f}}) - \nabla\mathbf{K}(\tilde{\mathbf{f}})(\mathbf{f} - \tilde{\mathbf{f}})\| \leq \rho C_R \|\nabla\mathbf{K}(\tilde{\mathbf{f}})(\mathbf{f} - \tilde{\mathbf{f}})\|.$$

Then we obtain

$$\|\nabla\mathbf{K}(\tilde{\mathbf{f}})(\mathbf{f} - \tilde{\mathbf{f}})\| \leq \frac{1}{1 - \rho C_R} \|\mathbf{K}(\mathbf{f}) - \mathbf{K}(\tilde{\mathbf{f}})\|,$$

if $\rho < 1/C_R$. Hence, (5.10) is proved. ■

A.9. Proof of Theorem 5.4.

Proof. By the definition of \tilde{H}_{n+1}^1 and $M(\mathbf{f})$, (4.4), and using (5.6), $\hat{\mathbf{u}} = 0$ and G convex, we obtain

$$\begin{aligned}
\langle \tilde{H}_{n+1}^1(\boldsymbol{\beta}^{n+1}), \boldsymbol{\beta}^{n+1} - \hat{\boldsymbol{\beta}} \rangle - \frac{1}{2} \|\boldsymbol{\beta}^{n+1} - \hat{\boldsymbol{\beta}}\|_{M_{n+2}^1 - M_{n+1}^1}^2 \\
\geq \|\mathbf{u}^{n+1}\|^2 + \langle \mathbf{K}(\hat{\mathbf{f}}) - \mathbf{K}(\mathbf{f}_\theta^{n+1}) - \nabla\mathbf{K}(\mathbf{f}_\theta^{n+1})(\hat{\mathbf{f}} - \mathbf{f}_\theta^{n+1}), \mathbf{u}^{n+1} \rangle \\
+ \langle [\nabla\mathbf{K}(\mathbf{f}_\theta^n) - \nabla\mathbf{K}(\mathbf{f}_\theta^{n+1})](\mathbf{f}^{n+1} - \mathbf{f}^n), \mathbf{u}^{n+1} \rangle.
\end{aligned}$$

Now we assume that $\mathbf{f}_\theta^{n+1} \in \mathcal{B}_{\tilde{\mathbf{f}}}(\rho_f)$ and $\mathbf{u}^{n+1} \in \mathcal{B}_{\hat{\mathbf{u}}}(\rho_u)$. Then by Lemma 5.3 and (5.8c), we have

$$\begin{aligned}
&\langle \mathbf{K}(\hat{\mathbf{f}}) - \mathbf{K}(\mathbf{f}_\theta^{n+1}) - \nabla\mathbf{K}(\mathbf{f}_\theta^{n+1})(\hat{\mathbf{f}} - \mathbf{f}_\theta^{n+1}), \mathbf{u}^{n+1} \rangle \\
&\geq -\eta \|\mathbf{K}(\hat{\mathbf{f}}) - \mathbf{K}(\mathbf{f}_\theta^{n+1})\| \|\mathbf{u}^{n+1}\| \\
&\geq -\frac{\eta}{\sigma_K} \|(\sigma_K + 1)\mathbf{u}^{n+1} - \mathbf{u}^n\| \|\mathbf{u}^{n+1}\| \\
&\geq -\left(\frac{\eta}{2\sigma_K} + \eta\right) \|\mathbf{u}^{n+1}\|^2 - \frac{\eta}{2\sigma_K} \|\mathbf{u}^{n+1} - \mathbf{u}^n\|^2.
\end{aligned}$$

By the global Lipschitz continuity in Theorem 5.1,

$$\langle [\nabla\mathbf{K}(\mathbf{f}_\theta^n) - \nabla\mathbf{K}(\mathbf{f}_\theta^{n+1})](\mathbf{f}^{n+1} - \mathbf{f}^n), \mathbf{u}^{n+1} \rangle \geq -\frac{5L\rho_u}{2} \|\mathbf{f}^{n+1} - \mathbf{f}^n\|^2 - \frac{L\rho_u}{2} \|\mathbf{f}^{n-1} - \mathbf{f}^n\|^2.$$

By Lemma 4.5 and (5.11), we obtain

$$\begin{aligned} \frac{1}{2} \|\boldsymbol{\beta}^{n+1} - \boldsymbol{\beta}^n\|_{M_{n+1}^1}^2 &\geq \frac{\kappa}{2\tau} \|\mathbf{f}^{n+1} - \mathbf{f}^n\|^2 + \frac{\|\mathbf{u}^{n+1} - \mathbf{u}^n\|^2}{2\sigma_K} \left(1 - \frac{\tau\sigma_K}{s(1-\kappa)} \|\nabla \mathbf{K}(\mathbf{f}_\theta^n)\|^2\right) \\ &\geq \frac{\kappa}{2\tau} \|\mathbf{f}^{n+1} - \mathbf{f}^n\|^2 + \frac{\eta}{2\sigma_K} \|\mathbf{u}^{n+1} - \mathbf{u}^n\|^2. \end{aligned}$$

Hence, arranging these terms yields that

$$\begin{aligned} \langle \tilde{H}_{n+1}^1(\boldsymbol{\beta}^{n+1}), \boldsymbol{\beta}^{n+1} - \hat{\boldsymbol{\beta}} \rangle - \frac{1}{2} \|\boldsymbol{\beta}^{n+1} - \hat{\boldsymbol{\beta}}\|_{M_{n+2}^1 - M_{n+1}^1}^2 + \frac{1}{2} \|\boldsymbol{\beta}^{n+1} - \boldsymbol{\beta}^n\|_{M_{n+1}^1}^2 \\ \geq \left(1 - \frac{\eta}{2\sigma_K} - \eta\right) \|\mathbf{u}^{n+1}\|^2 + \frac{\kappa - 5\tau L\rho_u}{2\tau} \|\mathbf{f}^{n+1} - \mathbf{f}^n\|^2 - \frac{L\rho_u}{2} \|\mathbf{f}^{n-1} - \mathbf{f}^n\|^2. \end{aligned}$$

Then by Theorem 4.4, we obtain

$$\begin{aligned} \text{(A.11)} \quad &\frac{1}{2} \|\boldsymbol{\beta}^0 - \hat{\boldsymbol{\beta}}\|_{M_1^1}^2 - \frac{1}{2} \|\boldsymbol{\beta}^{N+1} - \hat{\boldsymbol{\beta}}\|_{M_{N+2}^1}^2 \\ &\geq \left(1 - \frac{\eta}{2\sigma_K} - \eta\right) \sum_{n=0}^N \|\mathbf{u}^{n+1}\|^2 + \frac{\kappa - 5\tau L\rho_u}{2\tau} \|\mathbf{f}^{N+1} - \mathbf{f}^N\|^2 + \frac{\kappa - 6\tau L\rho_u}{2\tau} \sum_{n=0}^{N-1} \|\mathbf{f}^{n+1} - \mathbf{f}^n\|^2. \end{aligned}$$

Because of the assumptions on τ and σ_K in (5.11), we have

$$\|\boldsymbol{\beta}^0 - \hat{\boldsymbol{\beta}}\|_{M_1^1}^2 \geq \|\boldsymbol{\beta}^{N+1} - \hat{\boldsymbol{\beta}}\|_{M_{N+2}^1}^2.$$

Similar with the proof of Lemma 4.8, we claim sequence $\{\boldsymbol{\beta}^n\}_{n \in \mathbb{N}}$ is always in $O(\rho_f, \rho_u, \rho_v)$ and $\{\mathbf{f}_\theta^n\}_{n \in \mathbb{N}}$ is always in $\mathcal{B}_{\tilde{\mathbf{f}}}(\rho_f)$. Since (A.11) holds for all N , we have that $\{\mathbf{f}^n\}$ is a Cauchy sequence and $\mathbf{u}^n \rightarrow 0$. So $\mathbf{f}^n \rightarrow \tilde{\mathbf{f}}'$ when $n \rightarrow \infty$. Consequently, $\mathbf{K}(\tilde{\mathbf{f}}') = \mathbf{g}$, which is the desired result. \blacksquare

Acknowledgments. The authors would like to thank Buxing Chen, Dan Xia, Zhiqiang Xu, Zheng Zhang and Yunsong Zhao for their helpful discussions.

REFERENCES

- [1] R. E. Alvarez and A. Macovski. Energy-selective reconstructions in X-ray computerized tomography. *Phys. Med. Biol.*, 21(5):733–744, 1976.
- [2] R. Barber and E. Sidky. Convergence for nonconvex ADMM, with applications to CT imaging. Technical Report 2006.07278, ArXiv e-prints, 2021.
- [3] A. Beck. *First-Order Methods in Optimization*. Society for Industrial and Applied Mathematics, Philadelphia, PA, 2017.
- [4] A. Chambolle and T. Pock. A first-order primal-dual algorithm for convex problems with applications to imaging. *J. Math. Imaging Vision*, 40:120–145, 2011.
- [5] B. Chen, L. Xin, Z. Zhang, D. Xia, E. Sidky, and X. Pan. Optimization-based algorithm for solving the discrete x-ray transform with nonlinear partial volume effect. *Journal of medical imaging*, 7(5):053502, 2020.
- [6] B. Chen, Z. Zhang, D. Xia, E. Sidky, and X. Pan. Non-Convex Chambolle–Pock Algorithm for Multi-spectral CT. In *Proceedings of The Fifth International Conference on Image Formation in X-Ray Computed Tomography*, pages 377–381, 2018.

- [7] B. Chen, Z. Zhang, D. Xia, E. Sidky, and X. Pan. Non-convex primal-dual algorithm for image reconstruction in spectral CT. *Computerized Medical Imaging and Graphics*, 87:101821, 2021.
- [8] C. Chen, R. Wang, C. Bajaj, and O. Öktem. An Efficient Algorithm to Compute the X-ray Transform. *International Journal of Computer Mathematics*, DOI:10.1080/00207160.2021.1969017, 2021.
- [9] C. Clason, S. Mazurenko, and T. Valkonen. Acceleration and global convergence of a first-order primal-dual method for nonconvex problems. *SIAM Journal on Optimization*, 29(1):933–963, 2019.
- [10] M. Elad. *Sparse and Redundant Representations: From Theory to Applications in Signal and Image Processing*. Springer, 2010.
- [11] E. Esser, X. Zhang, and T. F. Chan. A General Framework for a Class of First Order Primal-Dual Algorithms for Convex Optimization in Imaging Science. *SIAM J. Imaging Sci.*, 3(4):1015–1046, 2010.
- [12] J. Fan and Y. Yuan. On the Quadratic Convergence of the Levenberg–Marquardt Method without Nonsingularity Assumption. *Computing*, 74(1):23–39, 2005.
- [13] B. He and X. Yuan. Convergence Analysis of Primal-Dual Algorithms for a Saddle-Point Problem: From Contraction Perspective. *SIAM J. Imaging Sci.*, 5(1):119–149, 2012.
- [14] B. Jin, Z. Zhou, and J. Zou. On the convergence of stochastic gradient descent for nonlinear ill-posed problems. *SIAM Journal on Optimization*, 30(2):1421–1450, 2020.
- [15] B. Kaltenbacher, A. Neubauer, and O. Scherzer. *Iterative regularization methods for nonlinear ill-posed problems*. Radon Series on Computational and Applied Mathematics. Walter de Gruyter, 2008.
- [16] G. Landi, E. Loli Piccolomini, and J. G. Nagy. A limited memory BFGS method for a nonlinear inverse problem in digital breast tomosynthesis. *Inverse Problems*, 33:095005 (21pp), 2017.
- [17] A. Macovski, R. E. Alvarez, J. L.-H. Chan, J. P. Stonestrom, and L. M. Zatz. Energy dependent reconstruction in X-ray computerized tomography. *Comput. Biol. Med.*, 6:325–336, 1976.
- [18] R. Rockafellar and R. Wets. *Variational Analysis*, volume 317. Springer-Verlag, 2004.
- [19] L. Rudin, S. J. Osher, and E. Fatemi. Nonlinear total variation based noise removal algorithms. *Physica D: Nonlinear Phenomena*, 60(1):259–268, 1992.
- [20] T. Valkonen. A primal-dual hybrid gradient method for nonlinear operators with applications to MRI. *Inverse Problems*, 30(5):055012 (45pp), 2014.
- [21] W. van Aarle, W. J. Palenstijn, J. Cant, E. Janssens, F. Bleichrodt, A. Dabravolski, J. De Beenhouwer, K. J. Batenburg, and J. Sijbers. Fast and Flexible X-ray Tomography Using the ASTRA Toolbox. *Optics Express*, 24(22):25129–25147, 2016.
- [22] Y. Wang and Z. Xu. Generalized phase retrieval: measurement number, matrix recovery and beyond. *Appl. Comput. Harmon. Anal.*, 47(2):423–446, 2019.
- [23] Y. Wang, W. Yin, and J. Zeng. Global Convergence of ADMM in Nonconvex Nonsmooth Optimization. *Journal of Scientific Computing*, 78:29–63, 2019.
- [24] Z. Wang, A. C. Bovik, H. R. Sheikh, E. P. Simoncelli, et al. Image quality assessment: from error visibility to structural similarity. *IEEE transactions on image processing*, 13(4):600–612, 2004.
- [25] Y. Zhao, X. Zhao, and P. Zhang. An extended algebraic reconstruction technique (E-ART) for dual spectral CT. *IEEE Transactions on Medical Imaging*, 34(3):761–768, 2015.